AD-A077 028 ILLINOIS UNIV AT URBANA-CHAMPAIGN DEPT OF ELECTRICAL --ETC F/G 4/1
MODEL COMPUTATIONS OF RADIO WAVE SCINTILLATION CAUSED BY EQUATO--ETC(U)
JUL 79 A W WERNIK F19628-78-C-0195
UNCLASSIFIED UILU-ENG-79-2555 AFGL-TR-79-0165 NL

1 OF 1
AD-
A077028



END
DATE
FILMED
12-79
DDC

AFGL-TR-79-0165

LEVEL II

12

MODEL COMPUTATIONS OF RADIO WAVE SCINTILLATION CAUSED BY EQUATORIAL BUBBLES

A. W. Wernik

Department of Electrical Engineering
University of Illinois at Urbana-Champaign
Urbana, Illinois 61801

July 1979

Scientific Report, No. 1

AD A077028

DDC
RECEIVED
NOV 21 1979
E

DDC FILE COPY

Approved for public release; distribution unlimited.

AIR FORCE GEOPHYSICS LABORATORY
AIR FORCE SYSTEMS COMMAND
UNITED STATES AIR FORCE
HANSCOM AFB, MASSACHUSETTS 01731

79 19 9 140

Qualified requestors may obtain additional copies from the Defense Documentation Center. All others should apply to the National Technical Information Service.

UNCLASSIFIED

SECURITY CLASSIFICATION OF THIS PAGE (When Data Entered)

REPORT DOCUMENTATION PAGE

READ INSTRUCTIONS BEFORE COMPLETING FORM

1. REPORT NUMBER: AFGL-TR-79-0165	2. GOVT ACCESSION NO.
3. RECIPIENT'S CATALOG NUMBER	
4. TITLE (and Subtitle): Model Computations of Radio Wave Scintillation Caused by Equatorial Bubbles	5. TYPE OF REPORT & PERIOD COVERED: No. 1 Scientific, July 1978 through July 1979
	6. PERFORMING ORG. REPORT NUMBER: TR No. 64, UILU-ENG-79-2555
7. AUTHOR(s): A. W. Wernik	8. CONTRACT OR GRANT NUMBER(s): F19628-78-C-0195
9. PERFORMING ORGANIZATION NAME AND ADDRESS: Department of Electrical Engineering, University of Illinois at Urbana-Champaign, Urbana, Illinois 61801	10. PROGRAM ELEMENT, PROJECT, TASK AREA & WORK UNIT NUMBERS: 63431F, 46430SAA
11. CONTROLLING OFFICE NAME AND ADDRESS: Air Force Geophysics Laboratory (PHP), Hanscom AFB, Massachusetts 01731, Monitor/Herbert E. Whitney/PHP	12. REPORT DATE: July 1979; NUMBER OF PAGES: 78
14. MONITORING AGENCY NAME & ADDRESS(if different from Controlling Office)	15. SECURITY CLASS. (of this report): UNCLASSIFIED
	15a. DECLASSIFICATION/DOWNGRADING SCHEDULE

16. DISTRIBUTION STATEMENT (of this Report)

Approved for public release; distribution unlimited.

17. DISTRIBUTION STATEMENT (of the abstract entered in Block 20, if different from Report)

UILU-ENG-79-2555, TR-64

18. SUPPLEMENTARY NOTES

Scientific rept. no. 1, Jul 78-Jul 79,

19. KEY WORDS (Continue on reverse side if necessary and identify by block number)

Equatorial scintillation
Ionosphere bubbles
Gigahertz scintillation
Parabolic equation

20. ABSTRACT (Continue on reverse side if necessary and identify by block number)

The apparent inhomogeneous nature of the equatorial electron density irregularities indicate that a new approach to the scintillation theory is required. Based on the available in situ electron density measurements and theoretical information a simple two-dimensional, deterministic model of the equatorial bubble is developed. The parabolic equation for a wave traversing such a bubble is solved numerically. The computed amplitude pattern suggests that wave diffraction on edges formed by sharp horizontal electron density gradients may be a possible cause of scintillation at gigahertz frequencies. Comparison with the

DD FORM 1 JAN 73 1473 EDITION OF 1 NOV 65 IS OBSOLETE

UNCLASSIFIED 276 009

SECURITY CLASSIFICATION OF THIS PAGE

20. Cont.

results obtained for a model of random irregularities with the same power spectrum shows that the medium characterized by sharp electron density gradients leads to stronger scintillation in a wide frequency range.

The amplitude pattern, scintillation index, frequency dependence and scatter plots computed for the model agree well with observations.

TABLE OF CONTENTS

		Page
1.	INTRODUCTION	1
2.	SUMMARY OF CURRENT EXPERIMENTAL AND THEORETICAL UNDERSTANDING OF EQUATORIAL IRREGULARITIES	3
3.	BASIS OF THE SCINTILLATION MODEL	8
	3.1 Parabolic Equation.	8
	3.2 Irregularity Model.	12
4.	NUMERICAL METHOD FOR SOLVING PARABOLIC EQUATION. .	15
5.	NUMERICAL RESULTS AND DISCUSSION	20
6.	CONCLUSIONS.	31
REFERENCES.		33
APPENDIX.		36

Accession For
NTIS GRA&I
DDC TAB
Unannounced
Justification
By
Distribution/
Availability Codes
Dist | Avail and/or special

TABLE OF CONTENTS

		Page
1.	INTRODUCTION	1
2.	SUMMARY OF CURRENT EXPERIMENTAL AND THEORETICAL UNDERSTANDING OF EQUATORIAL IRREGULARITIES	3
3.	BASIS OF THE SCINTILLATION MODEL	8
	3.1 Parabolic Equation.	8
	3.2 Irregularity Model.	12
4.	NUMERICAL METHOD FOR SOLVING PARABOLIC EQUATION. .	15
5.	NUMERICAL RESULTS AND DISCUSSION	20
6.	CONCLUSIONS.	31
REFERENCES.		33
APPENDIX.		36

1. INTRODUCTION

Recent activity in the equatorial scintillation studies was enhanced by the discovery of scintillating gigahertz frequency radio signals (Skinner et al., 1971) and by the new and fascinating experimental and theoretical results for the irregular structure of the equatorial ionosphere. Several papers reviewing equatorial scintillation phenomena and theory and measurements of equatorial irregularities were published recently by Farley et al., (1970); Basu and Kelley, (1977); Basu and Kelley (1979); Ossakow et al., (1979)). Interested readers should refer to these papers for more detailed references. In Section 2 only a brief summary of results pertinent to the future discussion is given. As will become evident, equatorial irregular structure can not be considered as random, mainly because of the presence of sharp gradients of electron concentration. Under such circumstances, a deterministic approach to scintillation is certainly more correct. The approach used in this report is based on the assumption of validity of the parabolic equation describing the complex wave amplitude for a wave propagating in a model irregular ionosphere. The model, which is deterministic, is based on the available satellite in-situ data and other experimental and theoretical information. It is described in Section 3. Section 4 and the Appendix discuss the numerical method, algorithm and computer program used to solve most efficiently the parabolic equation.

As shown in Section 5, modelling proved clearly the importance of the presence of sharp horizontal electron concentration gradients in producing strong scintillation of gigahertz frequency radio waves. Although the model is deterministic, some statistical parameters of radio waves have been computed, and frequency dependence of the scintillation index was found to be in good agreement with observations.

2. SUMMARY OF CURRENT EXPERIMENTAL AND THEORETICAL UNDERSTANDING OF EQUATORIAL IRREGULARITIES

Most information about the irregular structure of the equatorial ionosphere has come from back-scatter radar and in-situ satellite and rocket measurements. Several campaigns of simultaneous measurements of different types provided deeper insight into the nature of equatorial irregularities. Jicamarca back-scatter radar data show that 3-m size irregularities initially, right after sunset, occupy relatively thin layers below the F-layer peak which rapidly, sometimes in a matter of several minutes, thickens to several hundred kilometers extending well above the F-peak (Farley et al., 1970; Woodman and La Hoz, 1976). The extended irregular structures are called "plumes," which usually move with the velocity of the order of 100 ms^{-1}, occasionally exceeding 300 ms^{-1}. Simultaneous VHF scintillation measurements (Basu et al., 1977) show that as long as the irregular layer is thin scintillation intensity is low or moderate and the fading rate is small. However, the stage of fully developed plumes is accompanied by intense (>20dB on VHF) and rapid scintillation. At times of intense VHF scintillation, gigahertz frequency radio signals also scintillate. This scintillation is unexpectedly strong, exceeding 8 dB at 1.5 GHz and 4 dB at 4 GHz. Scintillation indices as large as 0.74 at 1.5 GHz and 0.63 at 4 GHz were reported (Taur, 1976). Evidently, in such cases, the weak scattering scintillation theory is not valid. Discussion of possible

causes of strong gigahertz frequency scintillation is one of the objects of this report.

It has been pointed out (Basu et al., 1978) that 3-m and km-size irregularities responsible for VHF scintillation coexisted only in the developing stage of plume, and in the later evening hours scintillation did not correlate with plumes. This led Basu et al. to speculate about the change of the cut-off scale size of the irregularity spectrum.

In-situ rocket and satellite measurements provided further information about equatorial irregularities. OGO-6 data showed that irregularities are usually associated with large depletions of the electron concentration known as bubbles (McClure et al., 1977). These bubbles move upward and westward with the velocity of the order of 150 ms^{-1} with respect to the background plasma (which at night rotates eastward). The observed east-west size of the bubbles ranges from 10 to several hundred kilometers and the depletions in bubbles up to three orders of magnitude were observed. Figure 1 illustrates the irregular structure inside the bubble. The very sharp gradients and the peaks are the most striking features. Similar structures have been observed below the F-peak during the rocket flights (Costa and Kelley, 1978). Costa and Kelley (1978) have shown that these kinds of structures have a one-dimensional power spectrum of the form k^{-2}, resembling the spectrum of turbulent-like irregularities. From the point of view of the scintillation theory, this is a very important result. The irregularity power spectrum plays a very important role in

the statistical theory of scintillation which makes use of the statistical properties of a medium to derive statistics of a scintillating wave. It is assumed that the irregularities are random and the background medium is homogeneous, or at least locally homogeneous. However, in the presence of sharp electron concentration gradients none of these two assumptions are exactly valid, and the scintillation theory based on other models may be more appropriate for the situation. Furthermore, mechanisms other than scattering and diffraction have been suggested to be efficient in producing scintillation (Crain et al., 1979). This point is discussed in more detail later on.

Recent simultaneous total electron content, airglow, and scintillation measurements provided further evidence that irregularities responsible for scintillation are associated with depletions in electron concentration (Koster, 1976; Weber et al., 1978; Yeh et al., 1979). This association is especially clear in the premidnight period.

Theoreticians were very successful in explaining the observed irregular structure of the equatorial ionosphere. The hierarchy of plasma instabilities suggested by Haerendel (1974) could produce a wide spectrum of observed irregularities. First in the hierarchy is the collisional Rayleigh-Taylor instability, which acts on the steep bottomside gradient of electron concentration and produces large-scale vertically oriented irregularities with sharp horizontal gradients. Favorable conditions for the cross-field instability are

created. This kind of instability leads to irregularities with wave-vectors oriented vertically and sizes roughly between 0.5 to 5 km. When the amplitude of these irregularities is large enough, the collisionless Rayleigh-Taylor instability becomes active and produces irregularities with sizes 50 to 500 m. Finally, kinetic drift waves can grow upon these irregularities after they reach large amplitudes. Irregularities generated by this mechanism will have sizes comparable to the ion gyro-radius (several meters).

Numerical simulation of the collisional Rayleigh-Taylor instability (c.f. Scannapieco and Ossakow, 1976; Ossakow et al., 1979) showed that originally bottomside plasma depletions can rise beyond the F peak. Figure 2 from Ossakow et al. (1979) shows the evolution of a bubble. Percentage depletion as large as 85% was reached and the rise velocity of the bubble was 160 ms^{-1}. Note the sharp electron concentration gradient on the leading edge of the bubble. An analytical model of uprising bubbles has been developed by Ott (1978) in the collision-dominated and the collisionless cases. Kelley and Ott (1978) showed that rising bubbles generate a wake with vortices. Originally, such vortices have a characteristic size of the order of the bubble size. In the presence of the background plasma density, gradient vortices will mix regions of differing density and create density irregularities with wavelengths both larger and smaller than the original size of the bubble. The power spectrum of density irregularities will be

proportional to k^{-1} for irregularities with sizes between the bubble size and the dissipation scale (~28 m for the case considered by Kelley and Ott). This seems to contradict the observed k^{-2} spectrum but, as pointed out by the authors, steepening of the spectrum is most likely due to the sharp edges of bubbles.

3. BASIS OF THE SCINTILLATION MODEL

The scintillation theory relates statistics of the wave parameters to statistics of the dielectric permittivity fluctuations ϵ_1 and, therefore, of electron concentration fluctuations. If dielectric permittivity fluctuations $\epsilon_1(\bar{\rho},z)$ can be considered as a Gaussian random field, then statistics of ϵ_1, and therefore of the complex amplitude, are completely determined by the first two moments of the field: its mean and autocorrelation function or structure function. If it is further assumed that the field is homogeneous, instead of the autocorrelation or structure function, the power spectrum can be used. This assumption is always made in the scintillation theory. It prevents us from considering the fields of ϵ_1 with sharp gradients, because in this case, ϵ_1 is certainly inhomogeneous. On the other hand, sharp electron concentration gradients are the most pronounced features of the irregular equatorial ionosphere. Consequently, some new approach to the scintillation is needed. In addition to that, sharp discontinuities in ϵ_1 can produce qualitatively new effects leading to scintillation (Crain et al., 1979).

In the rest of this section, the basis for the scintillation model free from assumptions on statistics of ϵ_1 is developed.

3.1 Parabolic Equation

A starting point for our consideration is the so-called parabolic equation (cf. Tatarski, 1971). For a wave propagating

in the z direction, it takes the form

$$-2ik \frac{\partial u}{\partial z} + \nabla_T^2 u + k^2 \varepsilon_1 u = 0 \qquad (3.1)$$

where u is the complex wave amplitude, $\varepsilon_1 = \varepsilon - \langle\varepsilon\rangle$ is the dielectric permittivity variation relative to some reference value $\langle\varepsilon\rangle$, ∇_T^2 is the transverse to the direction of propagation part of the Laplacian operator, and $k = 2\pi/\lambda$ is the wave number in the reference medium.

To apply (3.1) it is required (Tatarski, 1971) that:

(A) the characteristic scale of ε_1 variations is much larger than the wavelength.

(B) wave attenuation due to the presence of irregularities is small over a distance equal to the wavelength.

In addition, two sufficient conditions must be satisfied:

(C) the power reflected back is negligible,

(D) the Fresnel approximation is valid.

If conditions (A) - (D) are satisfied, equation (3.1) can be used in any medium, stochastic or deterministic. In the stochastic medium, the reference dielectric permittivity is simply the average value, while in the deterministic medium it can be any value. In our calculations $\langle\varepsilon\rangle$ has been chosen to be equal to 1, which is the value ε assumes outside the irregular region.

Condition (A) requires $\ell = \varepsilon_1 (\nabla\varepsilon_1)^{-1}$ to be much larger than the wavelength. Condition (D) is satisfied whenever (cf. Tatarski, 1971)

$$\frac{L}{k^3 \ell^4} << 1, \tag{3.2}$$

and, if only $k\ell<<1$, this inequality is valid even in the far zone where a distance L traversed by a wave is larger than $(k\ell)^{1/2}$.

Conditions (B) and (C) are much more difficult to discuss. To have some impression about the order of magnitude of wave attenuation in a deterministic medium, consider the case when ϵ_1 is a Gaussian function of x and y

$$\epsilon_1(x,y) = \epsilon_{10} \exp(-\rho^2/r^2) \qquad \bar{\rho}=(x,y) \tag{3.3}$$

and this irregularity extends throughout a distance L in the direction of propagation. Most of the attenuation results from the single scattering, therefore, if the power extracted from the incident wave by single scattering is small over a distance equal to the wavelength, the condition (B) is satisfied. Assuming that the Fresnel approximation is valid, a single scattered wave field is given by the equation:

$$u_1(\bar{\rho},L) = \frac{k^2 u_0}{4\pi} \int_0^L \frac{dz'}{L-z'} \iint_{-\infty}^{\infty} \epsilon_1(\bar{\rho}',z') \exp\left[-\frac{ik(\bar{\rho}-\bar{\rho}')}{2(L-z')}\right] d\bar{\rho}' \tag{3.4}$$

where u_0 is constant for a plane incident wave. For simplicity, we set $\bar{\rho}=0$, therefore, the upper estimate of the scattered power is obtained. Substituting (3.3) into (3.4), integrating and taking the absolute value of u_1 leads to the result

$$\frac{|u_1^2|}{u_0^2} = \frac{k^4 r^4 \varepsilon_{10}^2}{16} (\ell n^2 \rho + \phi^2), \qquad (3.5)$$

$$\rho^2 = 1 + (2L/r^2 k)^2, \quad \phi = \arctan(2L/r^2 k),$$

which is the fraction of the incident power attributed to a single scattering. The inverse of the extinction length d is obtained by dividing (3.5) by the slab thickness L. Extinction length is a measure of the wave attenuation. If $d^{-1}/k \ll 1$ condition (B) is satisfied.

Consider first the case $2L/kr^2 \ll 1$. It is easy to show that in this case

$$d^{-1}/k \approx kL\varepsilon_{10}^2/4. \qquad (3.6)$$

If (3.6) is multiplied and divided by $2kr^2$, the condition (B) can be written in the following form

$$\frac{k^2 r^2 \varepsilon_{10}^2}{8} \frac{2L}{kr^2} \ll 1. \qquad (3.7)$$

Note that an irregularity of size r causes the phase change $kr\varepsilon_{10}/2$. Therefore, inequality (3.7) means that for $2L/kr^2 \ll 1$, the condition (B) is satisfied even for large phase variations introduced by a single irregularity.

For $2L/kr^2 \gg 1$ the value of d^{-1}/k can be approximated by the following expression:

$$d^{-1}/k \approx \frac{k^4 r^4 \delta_{10}^2}{4} [\ell n(2L/kr^2)]^2 = k^2 L^2 \varepsilon_{10}^2 \left[\frac{\ell n(2L/kr^2)}{2L/kr^2}\right]^2 \qquad (3.8)$$

and the condition $d^{-1}/k \ll 1$ means that the total phase change $kL\varepsilon_{10}$ can not be exceedingly large.

To discuss condition (C) again, assume the Gaussian irregularity. One can expect that, whenever the scattering angle is small not too much power is reflected back. To estimate the scattering angle note that in the plane y=const it can be expressed in terms of the phase ϕ by

$$\alpha = \frac{1}{k} \frac{\partial \phi}{\partial x} \tag{3.9}$$

where $\phi = k\epsilon_1 L/2$. In our irregularity model, the scattering angle is maximum for y=0 and $x=r/\sqrt{2}$, where it assumes the value

$$\alpha_{max} = 0.46 \frac{L\epsilon_{10}}{r} = 0.46 \frac{kL\epsilon_{10}}{kr} \tag{3.10}$$

Condition (C) is satisfied provided $\alpha_{max} << 1$. It is clearly seen from (3.10) that with $kr >> 1$ this puts a limit on the total phase change.

With strong irregularities filling up the extended bubble structures, assumptions leading to the parabolic equation could be violated especially at lower frequencies. In fact, condition (B) is violated in our model calculations when scintillation at a frequency of 136 MHz is considered to be due to irregularities at the center of the well-developed bubble (Section 3.2). A rough estimate shows that in this case d^{-1}/k is larger than one for irregularities with the scale size smaller than 200 m.

3.2 Irregularity model

A parabolic equation can be solved numerically only if $\epsilon_1(\bar{\rho}, z)$ is known at each point of a three-dimensional space.

Because of the direct proportionality to electron concentration fluctuations ΔN, ε_1 can be determined provided ΔN is known from measurements. Unfortunately, satellite and rocket in-situ measurements give information only about ΔN along the satellite (rocket) path. Any attempt to obtain from these data a three-dimensional structure of irregularities would involve assumptions about their statistics. This is feasible if the data show randomness of ΔN. Figure 1 clearly shows that this is not the case: in addition to the large scale trend, sharp gradients of ΔN are present inside the bubble.

The two-dimensional model adopted for our calculation is very simple. It is assumed that at each height the horizontal relative variations of electron concentration $\Delta N/N$ are the same as those displayed in Figure 1. The concentration at the bubble's edge is taken as a reference. Allowance is made for its variations with the height and, in particular, the parabolic profile is adopted.

$$N(h) = N_0[1-(h-h_0)^2/H^2] \qquad (3.2.1)$$

where N_0 is the maximum electron concentration at the height h_0 and H is the scale height. In most cases we set h_0=350 km, $N_0=2.5\cdot10^5$ electrons cm^{-3} and H=110 km.

As was noticed in Section 2 theoretical simulations show that in the course of the bubble development its leading edge becomes sharper while the trailing edge seems

to be more blunt. To take this into account (3.2.1) is multiplied by some weighting function. The weighting function corresponding to what we call initial stage is shown in Figure 3a, while Figure 3b displays the weighting function for the developed stage of the bubble.

The model, is summarized in Figures 4a and 4b, which show electron concentration variations ΔN at several levels inside the bubble for the initial and developed stages, respectively.

Our model is far from being perfect. In particular it does not take into account small-scale vertical variations of the electron concentration. But at least it is free from any assumptions about the statistics of ΔN and should correctly answer the question about the role of vertically extended sharp gradients in producing scintillation.

4. NUMERICAL METHOD FOR SOLVING PARABOLIC EQUATION

The parabolic equation (3.1) can be solved analytically only for a very few simple forms of the function $\varepsilon_1(\bar{\rho},z)$. A general numerical approach is needed. We are interested in solving (3.1) when the dielectric permittivity is a function of x and z only, thus, $\nabla_T^2=\partial^2/\partial x^2$. For a plane incident wave the initial value for this equation is u(x,0)=const=1. The change of variables t=kz, ξ=kx leads to the equation

$$\frac{\partial u}{\partial t} + \frac{i}{2}\frac{\partial^2 u}{\partial \xi^2} + \frac{i}{2}\varepsilon_1(\xi,t)u = 0 \qquad (4.1)$$

Basically, two methods for the numerical treatment of parabolic equations exist: explicit and implicit method (cf. Ames, 1969). Although the explicit method is very simple and does not involve the troublesome solution of a large set of equations, it gives a somewhat imperfect model for a parabolic equation (Ames, 1969), and places a stringent restriction on the step-size in the t-direction. Because of this, we have chosen as an implicit scheme a special case which is the well-known Crank-Nicholson difference scheme. A thorough discussion of the stability condition, truncation error and convergence has been made by Crandall (1955) (see also Ames, 1969) for the diffusion equation and for a special case of the equation analogous to (4.1) by Borodziewicz (1978). The scheme makes use of the following analog to the second derivative:

$$\frac{\partial^2 u}{\partial \xi^2} = \frac{1}{h^2}\left[\sigma\left(u_{k+1}^{n+1} - 2u_k^{n+1} + u_{k-1}^{n+1}\right) + (1-\sigma)\left(u_{k+1}^{n} - 2u_k^{n} + u_{k-1}^{n}\right)\right], \tag{4.2}$$

where $u_k^n = u(kh, n\tau)$ with h and τ being the step sizes in the ξ and t directions, respectively, and $0 \leq \sigma \leq 1$ is a weighting factor. The term $\partial u/\partial t$ is approximated by

$$\left(u_k^{n+1} - u_k^n\right)/\tau, \tag{4.3}$$

and the term $\varepsilon_1 u$ by

$$\frac{\varepsilon_{1k}^{n+1} + \varepsilon_{1k}^{n}}{2}\left[\sigma u_k^{n+1} + (1-\sigma)u_k^n\right]. \tag{4.4}$$

If $\sigma=0$ the explicit scheme is obtained, while $\sigma=1/2$ results in the Crank-Nicholson scheme. In general, increased σ improves stability and convergence of the solution for a given value of $r=\tau/h^2$. If $\sigma \geq 1/2$, the solution is absolutely stable for all τ, and if $\sigma=1$, the solution is absolutely stable and convergent. For the heat transfer equation, a minimum truncation error of the order of $O(h^4)$ is attained for

$$r = \frac{1}{\sigma(1-2\sigma)}. \tag{4.5}$$

Otherwise, the truncation error is of the order of $O(h^2)$. We see that the Crank-Nicholson scheme requires an infinitely large value of r to reach minimum error. For equation (4.1)

no corresponding relation was derived. However, computer runs showed that a satisfactory compromise between the error and convergence is attained if $\sigma=0.51$ and $0.5\leq r\leq 2.5$.

Substitution of (4.2), (4.3) and (4.4) into the parabolic equation (4.1) leads to the following difference equation:

$$\frac{i\tau}{2h^2}\,\sigma u_{k+1}^{n+1}+\left(1-\frac{i\tau}{h^2}\,\sigma+\frac{i\tau}{2}\,\sigma f_k^n\right)u_k^{n+1}+\frac{i\tau}{2h^2}\,\sigma u_{k-1}^{n+1}=$$

$$-\frac{i\tau}{h^2}(1-\sigma)u_{k+1}^n+\left[1+\frac{i\tau}{h^2}(1-\sigma)-\frac{i\tau}{2}(1-\sigma)f_k^n\right]u_k^n$$

$$-\frac{i\tau}{2h^2}(1-\sigma)u_{k-1}^n, \qquad (4.6)$$

$$k=\pm 1,\ \pm 2,\ \ldots\ \pm K$$

$$n=0,\ 1,\ 2,\ \ldots\ N$$

where $f_k^n=(\varepsilon_{1k}^{n+1}+\varepsilon_{1k}^n)/2$.

In the discrete scheme the initial value $u(x,0)=1$ is written $u_k^0=1$. Because of the assumed symmetry of $\varepsilon_1(x,z)$ with respect to the z axis, $u_{-k}^n=u_k^n$, and the system (4.6) of 2K equations reduced to the system of K equations. It contains K+2 unknowns u_k^n with K unknowns of interest to us ($k=1,2,\ldots,K$), and two unknowns u_0^n and u_{k+1}^n beyond the boundaries of the considered region. The usual procedure is to introduce the so-called "false" boundaries at k=0 and k=K+1. If the derivatives of u at the "true" boundaries are known these "false" boundaries can be easily derived.

We set $u_0^n=0$ and $u_{k+1}^n=0$ which introduces some discontinuities. As noticed by Ames (1969), if the stable scheme is used, the effect of such discontinuities does not penetrate deeply into the field of integration. In this way, the system (4.6) becomes tridiagonal with K unknowns. It can be written in the matrix form

$$B^n U^{n+1} = (B^n - \tau A^n) U^n, \qquad n=0,1,2,\ldots,N \tag{4.7}$$

where U^h is the column matrix with u_k^n as elements. Matrices A^n and B^n are tridiagonal with the following elements:

$$A^n_{k,k} = -\frac{i}{h^2} + \frac{i}{2} f^n_k \qquad A^n_{k+1,k} = A^n_{k,k+1} = \frac{i}{2h^2} \qquad k=1,2,\ldots,K$$

$$A^n_{kj}=0 \qquad \text{for } k\neq j \quad k\neq j+1 \tag{4.8}$$

$$B^n_{k,k} = 1-i\tau\sigma\left(\frac{1}{h^2} - \frac{f^n_k}{2}\right) \qquad B^n_{k+1,k} = B^n_{k,k+1} = \frac{i\tau\sigma}{2h^2} \qquad k=1,2,\ldots,K$$

$$B^n_{k,j}=0 \qquad \text{for } k\neq j \quad k\neq j+1 \tag{4.9}$$

The solution of the matrix equation (4.7) is

$$U^{n+1} = U^n - (B^n)^{-1} \tau (A^n U^n) \tag{4.10}$$

To get the second term on the right-hand side of (4.10), A^n is first multiplied by U^n, already known from the previous step, and then the matrix equation $B^n X = A^n U^n$ is solved. Because B^n is tridiagonal, the matrix inversion can be

avoided by using the Gaussian elimination. The so-called Thomas algorithm is most often used. The system of equations is written in the form

$$a_k x_{k-1} + c_k x_k + b_k x_{k+1} = d_k \qquad k = 2,3,\ldots, K-1$$

$$c_1 x_1 = -b_1 x_2 + d_1 \tag{4.11}$$

$$c_K x_K = -a_K x_{K-1} + d_K$$

The solution is assumed to be in the form

$$x_k = \alpha_{k+1} x_{k+1} + \beta_{k+1} \tag{4.12}$$

where

$$\alpha_2 = -a_1/c_1 \qquad \beta_2 = x_1/c_1$$

$$\alpha_{k+1} = \beta_k/(a_k\alpha_k + c_k) \tag{4.13}$$

$$\beta_{k+1} = (d_k - a_k\beta_k)/(a_k d_k + c_k)$$

Noting that $x_K = \beta_{K+1}$ the unknowns x_k are successively found from (4.12). It has been shown that this scheme does not introduce large errors due to round-off errors in the calculations (Ames, 1969) and is very efficient in terms of computer time.

A complete program for solving the parabolic equation is given in the Appendix.

5. NUMERICAL RESULTS AND DISCUSSION

The parabolic equation (3.1) has been solved for a model equatorial plasma bubble filled with irregularities whose horizontal structure is the same as the one measured in-situ by McClure et al. (1977) and shown in their Figure 7. The satellite altitude was approximately 280 km and probably did not change appreciably during the passage through a bubble whose horizontal size was $\sim$50 km. The F-peak height at the time of the measurements was approximately 400 km.

After enlargement, the curve in Figure 7 of McClure et al. was digitized every 42 m which is approximately 10 m less than the sampling interval of in-situ measurements. This sets the lower limit on the irregularity scale-size or the scale length of the electron density gradient. It is still much less than the Fresnel zone dimension for a typical distance between the bottom-side of the irregular layer and the receiver (200-300 km) and the highest wave frequency considered in this report, which is 6 GHz.

To have some impression about the irregularity spectrum, the digitized data were high-pass filtered to remove any components larger than 10 km and the power spectrum was computed. Figure 5 shows that the spectral amplitude roughly follows the κ^{-1} law except for the extreme point at the low frequency part of the spectrum. This is a very typical spectrum of ionospheric F region irregularities (Dyson et al., 1974).

We assumed that the relative electron density fluctuations at each height inside a bubble follow the same horizontal pattern as one given in Figure 1. The background density is parabolic as described in Section 2. With the weighting function corresponding to the "initial stage" of a bubble, before it rose above the F-peak, the horizontal absolute electron density variation ΔN at four different levels inside the bubble is given in Figure 4a. The largest $\Delta N = 1.7 \cdot 10^5$ electrons$\cdot$cm^{-3} is reached close to the center of the bubble. If the bubble thickness L is defined as a distance between levels at which the weighting function falls to e^{-1}, we have L=30 km.

The second extreme case to be discussed corresponds to the "developed stage" of a bubble (Figure 4b). In this case, the maximum ΔN is approximately equal to $2 \cdot 10^5$ electrons$\cdot$cm^{-3} and the bubble thickness L=115 km.

The scintillation pattern resulting from our computations for a wave of frequency 1.5 GHz passing through the initial stage bubble is shown in Figure 6. The real and imaginary components of the complex amplitude as well as amplitude and phase in π units are depicted. The most interesting feature is the correspondence between the position of strong amplitude outbursts and the location of sharp electron density gradients in Figure 1. This seems to suggest the refractive scattering mechanism proposed by Crain et al. (1979) as a cause of appreciable scintillation. However, as we show later in this section the diffraction on edges

more easily explains the obtained feature. It is also interesting to note one more striking peculiarity, namely, the weak dependence of the amplitude outbursts on the absolute value of electron density deviation ΔN.

For a developed, thick bubble the edge effect is largely obscured by amplitude fluctuations attributed to scattering or diffraction by smoother structure (Figure 7). Nevertheless, stronger amplitude scintillation can still be noted close to sharp gradients of ΔN. On lower frequencies the edge effect can hardly be distinguished from scattering (Figure 8b). However, its presence can be seen from Figure 8a, which shows the amplitude pattern at 300 km height, i.e., inside the bubble. Evidently, the edge diffraction develops amplitude fluctuations at shorter distances than does the scattering.

To discuss further the effect of an isolated sharp gradient in electron density, we assumed a wave passing through a one-dimensional screen which at the point $x=x_0$ changes the wave's phase from 0 to some constant value ϕ_0. The complex amplitude at a distance z is given by

$$u(x,z) = \sqrt{\frac{k}{2\pi i z}} \int_{-\infty}^{\infty} u(x',0)\exp\left[ik\,\frac{(x-x')^2}{2z}\right]dx', \tag{5.1}$$

where

$$\begin{aligned} u(x,0) &= e^{i\phi_0} \quad \text{for } x>x_0 \\ &= 1 \quad\;\; \text{for } x<x_0 \end{aligned} \tag{5.2}$$

Simple integration and separation of the real and imaginary parts of u(x,z) lead to the following formulae

$$\text{Re } u(x,z) = \cos^2 \frac{\phi_0}{2} - \frac{1}{2}\{[1-\sqrt{2}\cos(\frac{\pi}{4} - \phi_0)]C(\alpha) + [1-\sqrt{2}\sin(\frac{\pi}{4} - \phi_0)]S(\alpha)\}, \quad (5.3)$$

$$\text{Im } u(x,z) = \frac{1}{2}\sin\phi_0 - \frac{1}{2}\{[1-\sqrt{2}\cos(\frac{\pi}{4} - \phi_0)]S(\alpha) - [1-\sqrt{2}\sin(\frac{\pi}{4} - \phi_0)]C(\alpha)\}, \quad (5.4)$$

where $S(\alpha)$ and $C(\alpha)$ are the Fresnel integrals of the argument $\alpha=(x-x_0)\sqrt{k/2z}$. Equations (5.3) and (5.4) were used to obtain the diffraction pattern at a distance z=350 km from a screen for frequencies of 360 MHz and 4 GHz with ϕ_0=16.4 and 1.48, respectively. The sudden phase jump was put at x=3 km. Results of the calculations are shown in Figure 9. A typical oscillatory pattern can be noticed. Oscillations are much faster at 4 GHz and dumped at shorter distances from the discontinuity, therefore, the edge effect is more localized in this case than at lower frequency. This explains why at higher frequencies it is easier to find the correspondence between sharp electron density gradients and the characteristic wave amplitude pattern. At lower frequencies the effect of closely spaced sharp gradients leads to a rather complicated picture not resembling the pattern produced by localized discontinuities. Thus, the edge effect is not seen in Figure 8b.

Crain et al. (1979) suggested the refractive scattering mechanism as a possible cause of scintillation at gigahertz frequencies. This mechanism involves a total internal

reflection from vertically extended horizontal discontinuities of electron density. Under some strict conditions imposed on the slope of discontinuity, the direct wave interferes with the unattenuated, reflected wave leading to strong amplitude fluctuations. A thorough discussion of the mechanism would require ray tracing in the model bubble with sharp boundaries. However, if the maximum grazing angle is small the parabolic equation offers an adequate mathematical description of the effect. Thus, we might expect that our calculations take into account refractive scattering. To check the importance of refractive scattering relative to the diffraction on edges, we computed the diffraction pattern produced by a screen which changes the phase of the wave proportionally to ΔN given by in-situ data. The proportionality constant was chosen such as to achieve the best agreement between the phase variations at a distance of 350 km from a screen with those at a distance 400 km from the top of a bubble when the full model is used. We wish to note at this point that the phase screen was placed not in the middle of the scattering layer (approximately 300 km height) but above the layer (cf. Figure 3a). This was necessary in order to make allowance for the development of amplitude scintillation as strong as that given by the solution of the parabolic equation. This remark might be of some importance to those who use the strong phase screen theory in interpreting the data.

Figures 10 and 11 present the comparison of the amplitude and phase variations at 360 and 4000 MHz as produced

by the phase screen and the initial stage model bubble. Close inspection of the figures indicates a remarkable similiarity between amplitude and phase structures with only slightly deeper fading at 360 MHz produced by the bubble. We conclude that at least to the order of approximation given by the parabolic equation the refractive scattering is either of no importance as compared to the edge diffraction effect or both effects are indistinguishable.

In Figures 12 and 13 we present the amplitude fluctuations at several frequencies for the initial and developed stages of the bubble, respectively. The edge effect is clearly seen on gigahertz frequencies in the developed stage and even at 800 MHz in the case of the initial bubble stage. It is interesting to note an increase in the fading rate as the bubble thickens. This is clearly seen at all frequencies except at 4 GHz which is dominated by the edge effect. This agrees very well with measurements (Basu et al., 1977) showing rising amplitude fading rate when the bubble develops and extends above the F-peak. At the outskirts of the bubble (distance larger than 15 km), scintillation intensity and fading rate are smaller than those closer to the center, mainly due to the deficiency of small scale electron density irregularities. The fading rate, which is also changing with frequency, is usually larger at lower frequencies. This is in agreement with observations by Rino et al., (1978) but contrary to the weak scatter

scintillation theory which predicts the dominant fading period proportional to the Fresnel zone size $\sqrt{\lambda z}$. However, when scintillation is strong, as in our case at frequencies below 4 GHz, the multiple scattering effects reduce the characteristic size of the wave field fluctuations leading to the increase of the fading rate (Yeh et al., 1975). The practical importance of the scintillation index justifies its calculations in spite of the obvious nonstationarity of the computed amplitude pattern noticeable especially at higher frequencies. The S_4 scintillation index was calculated only for the segment of data from x=0 to 15 km. The segment of x=15 to 25 km shows clearly a different amplitude structure due to the lack of small-scale electron density irregularities. Between x=0 and 15 km, scintillation indices calculated for each 5 km data segment differed not more than 25% which gives the impression about the stationarity assumption. The frequency dependence of scintillation index is shown in Figure 14. For moderately strong scintillation ($S_4<0.5$), S_4 is proportional to $f^{-\nu}$ with ν between 1 and 1.5. However, the index ν is closer to 1.5 for the scintillation index smaller than 0.2. As one would expect, the stronger the scintillation the weaker is its frequency dependence. We must point out, however, that at low frequencies the assumptions leading to the parabolic equation might break down. In fact, at 136 MHz in the case of a thick, developed bubble, the average intensity is about 15% lower than the intensity of the incident wave. This means that 15% of the

incident power is backscattered from the irregular layer, which no longer is small. In other cases under consideration, the backscattered power was less than 10% of the incident power. Figure 15 shows the case when the average signal level close to the center of the bubble is much below the level of the incident wave. In this particular example, only about 77% of the power is transmitted through the bubble. The result shown in Figure 15 was for frequency wave of 136 MHz passing through the extended bubble and the F-peak electron density was $3.5 \cdot 10^5$ electrons$\cdot$cm^{-3}. It would be interesting to examine the observational data to find cases where strong scintillation is accompanied by a decrease in the signal level. If such cases could be found, this would indicate the need for modification of the scintillation theory based on the parabolic equation.

It is interesting to compare the scintillation pattern produced by a bubble with sharp electron density gradients to that given by a bubble with random irregularities. To do that the electron density profile shown in Figure 1 was low-pass filtered with the cut-off wave number 0.1 km^{-1}. The high-frequency component of the data was obtained by subtracting low-frequency part from the original data. The high-frequency component of the data was then Fourier analyzed and the amplitude and phase of each Fourier component was determined. Following the procedure used by Costa and Kelley (1978) a random phase angle was added to

each phase, the data were then transformed back to the spatial domain and added to the low-frequency component of the original data. As a result we obtained the electron density profile with random high-frequency component which has the same power spectrum and variance of the electron density as the high-frequency component of the original data. Two examples of such profile generated using different random numbers are shown in Figures 16a and 16b. Note that sharp spikes and gradients clearly seen in Figure 1 are not present on these profiles. On the other hand, they contain more weak, small-scale structures.

The scintillation pattern produced by the "initial stage" bubble with horizontal electron density profiles as shown in Figures 16 was calculated leading to the result shown in Figure 17. At 4 GHz almost no scintillation is seen. The weakness of scintillation is confirmed by the calculated scintillation index of 0.02 for both runs. This is approximately half of the scintillation index calculated when the original profile is used. The variance of the high-frequency electron density component is equal to $6.6 \cdot 10^3$ electrons$\cdot$cm^{-3} which is only slightly smaller than that for the original data ($7.7 \cdot 10^3$ electrons$\cdot$cm^{-3}). Thus the two-fold decrease in the scintillation index can not be explained by the difference in $\langle(\Delta N)^2\rangle$ since in the weak scattering scintillation theory the scintillation index S_4 is directly proportional to $\langle(\Delta N)^2\rangle^{1/2}$. Therefore, random electron density fluctuations would have to be stronger (in our case two times stronger) to give scintillation as strong as that

produced by a medium dominated by sharp electron density gradients. Also at lower wave frequencies the scintillation index is enhanced by the presence of sharp electron density gradients. For instance, at 360 MHz for the original electron density profile S_4=0.64 while the randomized profiles lead to S_4=0.45 and 0.52, for run A and B, respectively. Obviously, the difference between the scintillation indices is smaller than at higher frequencies because of the effect of strong scattering which reduces the scintillation index dependence on $\langle \Delta N^2 \rangle$.

Sometimes observational data are represented in the form of scatter plots on the plane Imu-Reu. For completeness, we show in Figure 18 several such plots, all of them obtained using the same "initial stage" bubble model and differing in the wave frequency only. No filtering to separate the focus and scatter components was applied mainly because of the nonstationarity of the imaginary and real parts of the complex amplitude and difficulty in choosing the appropriate cut-off wave number. Nevertheless, it is interesting to note the obvious similarity between the model plots and plots derived from the scintillation data (cf. Fremouw et al., 1978). Both the model and data show a clear change from the phase dominated scintillation at high frequencies to the dominance of the scatter component with the power evenly distributed between Imu and Reu at lower frequencies.

In our model we have assumed that the relative electron density fluctuation $\Delta N/N$ does not depend on the height inside

a bubble. This assumption leads to the exaggerated phase fluctuations and possibly also to the overestimated scattering effects in amplitude. However, the edge diffraction effect is correctly predicted.

6. CONCLUSIONS

Solution of the parabolic equation for the complex amplitude of a wave passing through a simple model of an equatorial bubble revealed the importance of sharp horizontal gradients of the electron density in producing scintillation effects. Preliminary discussion of the effects suggests the diffraction on edges formed by sharp gradients as a possible mechanism of scintillation. The edge effect is particularly important at higher gigahertz frequencies where it is not obscured by scattering. The important fact is that the edge diffraction leads to appreciable scintillation even if ΔN is quite moderate and L is small.

The computed amplitude scintillation pattern is in good agreement with the observations, which indicate an increase of the scintillation rate with the increase of the bubble thickness and show a change in the scintillation rate from slow, close to the edges of the bubble, to fast, at its center. The frequency dependence of scintillation is of the type $f^{-\nu}$ with ν between 1 and 1.5 at gigahertz frequencies. There is a tendency toward smaller values of ν as the bubble thickens.

The bubble model we have used is deterministic. Due to the obvious nonhomogeneity of electron density fluctuations, it is difficult to compare the obtained results with those based on the statistical scintillation theory. Nevertheless, we have shown that the model of random irregularities

characterized by the same power spectrum as the medium with sharp electron density gradients produces less scintillation not only at GHz frequencies but also at lower frequencies where the scattering effects should be dominating. Apparently, the increased strength of scintillation can be attributed to the diffraction on sharp edges--the scintillation mechanism which is not taken into account by the statistical scintillation theory.

REFERENCES

Ames, W. F., Numerical Methods for Partial Differential Equations, Barnes & Noble, Inc., New York, 1969.

Basu, S., J. Aarons, J. P. McClure, C. LaHoz, A. Bushby, and R. F. Woodman, "Preliminary Comparisons of VHF Radar Maps of F-region Irregularities with Scintillations in the Equatorial Region", J. Atmos. Terr. Phys., v.39, pp.1251-1261, 1977.

Basu, S., and M. C. Kelley, "Review of Equatorial Scintillation Phenomena in Light of Recent Developments in the Theory and Measurements of Equatorial Irregularities," J. Atmos. Terr. Phys., v.39, pp.1229-1242, 1977.

Basu, S., and M. C. Kelley, "A Review of Recent Observations of Equatorial Scintillations and Their Relationships to Current Theories of F-region Irregularity Generation," Radio Sci., (in press, 1979).

Basu, S., S. Basu, J. Aarons, J. P. McClure and M. D. Cousius, "On the Coexistence of Kilometer-and Meter-Scale Irregularities in the Night-time Equatorial F Region," J. Geophys. Res., v.83, No.A9, pp.4219-4226, 1978.

Borodziewicz, W., "Approximate Solution of the Equation for the Second Moment of the Wave Function," (Unpublished manuscript) Space Research Center, Polish Academy of Sciences, Warsaw, Poland, 1978.

Costa, E., and M. C. Kelley, "On the Role of Steepened Structures and Drift Waves in Equatorial Spread F." v.83, J. Geophys. Res., v.83, No.A9, pp.4359-4364, 1978.

Crandall, S. H., "An Optimum Implicit Recurrence Formula for the Heat Conduction Equation," Quart. App. Math., v.13, pp.318-320, 1955.

Crain, C. M., H. G. Booker, and J. A. Ferguson, "Use of Refractive Scattering to Explain SHF Scintillation", Radio Sci., v.14, pp.125-134, 1979.

Dyson, P. L., J. P. McClure, and W. B. Hanson, "In situ Measurements of the Spectral Characteristics of F Region Ionospheric Irregularities", J. Geophys. Res., v.79, pp.1497-1502, 1974.

Farley, D. T., B. B. Balsley, R. F. Woodman, and J. P. McClure, "Equatorial Spread F: Implications of VHF radar observations," J. Geophys. Res., v.75, 7199, 1970.

Haerendel, G., "Theory of equatorial spread-F", Preprint, Max-Planck-Institut für Physik und Astrophysik, Garching, W. Germany, 1974.

Kelley, M. C., and E. Ott, "Two-Dimensional Turbulence in Equatorial Spread F," J. Geophys. Res., v.83, pp.4369-4372, 1978.

Koster, J. R., "Study of the Equatorial Ionosphere," Report AFGL-TR-77-0165, University of Ghana, Legon, Ghana, 1976.

McClure, J. P., W. B. Hanson and J. H. Hoffman, Plasma bubbles and irregularities in the equatorial ionosphere, J. Geophys. Res., v.82, 2650-2656, 1977.

Ossakow, S. L., S. T. Zalesak and B. E. McDonald, and P. K. Chaturvedi, "Nonlinear Equatorial Spread F: Dependence on the Altitude of the F Peak and Bottomside Background Electron Density Gradient Scale Length," J. Geophys. Res., v.84, pp.17-23, 1979.

Ott, E., "Theory of Rayleigh-Taylor Bubbles in the Equatorial Ionosphere," J. Geophys. Res., v.83, pp.2066-2070, 1978.

Scanapieco, A. J., and S. L. Ossakow, "Nonlinear Equatorial Spread F," Geophys. Res. Letts., v.3, p.451, 1976.

Skinner, N. J., R. F. Kelleher, J. B. Hacking, and C. W. Benson, "Scintillation Fading of Signals in the SHF Band", Nature, v.232, p.19, 1971.

Rino, C. L., R. A. Long, M. D. Cousins, and R. C. Livingston, "Continued Performance of the Wideband Satellite Experiment", Bimonthly Progress Report #5, SRI International Project 6436, SRI International, Menlo Park, CA. 94025, 1978.

Tatarski, V. I., "The Effects of the Turbulent Atmosphere on Wave Propagation", U.S. Department of Commerce, National Technical Information Service, Springfield, Va., 1971.

Taur, R. R., "Simultaneous 1.5 and 4 GHz Ionospheric Scintillation Measurements", Radio Sci., v.11, pp.1029, 1976.

Weber, E. J., J. Buchau, R. H. Eather, and S. B. Mende, "North/South Aligned Equatorial Airglow Depletions," J. Geophys. Res., v.83, pp.712-716, 1978.

Woodman, R. F., and C. LaHoz, "Radar Observations of F Region Equatorial Irregularities," J. Geophys. Res., v.81, p.5447, 1976.

Yeh, K. C., C. H. Liu and M. Y. Youakim, "A Theoretical Study of the Ionospheric Scintillation Behavior Caused by Multiple Scattering", Radio Sci., v.10, pp.97-106, 1975.

Yeh, K. C., H. Soicher, and C. H. Liu, "Observations of Equatorial Ionospheric Bubbles by the Radio Propagation Method," J. Geophys. Res. (in press, 1979).

APPENDIX

In this appendix the algorithm and computer program (in CDC FORTRAN Extended) used to solve the two-dimensional parabolic equation (4.1) are given. The employed method is described in Section 4.

The program was made versatile to be used with an arbitrary model of the irregular ionosphere, but also to make possible calculations for a wave which propagates in a free space after traversing an irregular layer or a wave disturbed by a phase changing screen.

The input parameters are:

K - number of steps in the horizontal x direction,

N - number of steps in the vertical z direction,

TAU - step-size in the z direction (in m),

H - step-size in the x direction (in m),

SIGM - weighting factor (our choise was SIGM=0.51),

FREQ - wave frequency (in MHz),

N1 - N1=1 for the phase screen model,

KSKIP - number of steps in the z direction recorded on the file PASS (which is the renamed file RESULT) over which one has to skip to get to the z level from which further computations will be made. This is used whenever one wants to continue computations with the changed step-size TAU, or when further computations are to be made outside a scattering medium.

XM - only every XM step in the z direction is recorded on files RESULT and TERM

KK - only every KK step in the x direction is recorded on file TERM.

IC - used as an indicator. If IC=1 computations are made inside the scattering medium, if IC=0, for computations outside a medium and for the phase screen model.

KL - total number of steps in the z direction calculated in the previous runs. KL is used to calculate the overall distance passed by a wave.

NP - used as the reading indicator. If NP>0 input parameters recorded on the file PASS are read. Otherwise it is assumed that they were not recorded.

K2 - K2=0 if the input file ELFL must be read. It does not need to be read for computations outside a scattering medium, but must be read at the beginning of the phase screen computations.

PHLØ - phase variance or a constant converting data stored on ELFL to phase variations.

The above parameters are universal and must be supplied whenever the program is used. Below, the described parameters which apply only to the model of a plasma bubble discussed in the report:

AL and ZO - weighting function at the top of a bubble is changing according to EXP(-((Z-ZO)/AL)**2)

BET and ZOO - weighting function at the bottom of a bubble is changing according to EXP(-((Z-ZOO)/BET)**2. For Z.GE.ZO and Z.LE.ZOO the weighting function is constant and equal 1.

ZMAX - height of the F-peak measured

ELMAX - electron density at the F-peak in electrons·cm^{-3}

ELZ - electron density at Z=0 in electrons·cm^{-3}.

Note that Z=0 corresponds to a height at which computations start. All distances are in meters.

All input parameters are read from the file DA2. Horizontal variations in a medium or on a phase screen are given

in arbitrary units and read from the file ELFL. Results of computations are written on the files RESULT and TERM. RESULT contains high-accuracy results intended to be used for plotting or further calculations. In the later case this file must be renamed to PASS and will be read during the next program run. TERM is used only for printing purposes and has the same content as RESULT.

Instead of using the COMPLEX variables the program uses the matrix representation of complex variables with the first column being the real part and the second column the imaginary part of a variable.

Subroutine YO sets the initial values to the matrix representing the complex amplitude. If the phase screen model is used, subroutine YO1 sets values of the complex amplitude on the screen. If KSKIP.NE.0 initial values are read from PASS.

Using the model of irregularities, subroutine FLUCT calculates dielectric permittivity fluctuation and its mean value at two adjacent z levels.

Both A and B matrices of equation (4.7) are stored in the form of three matrices: A, B, and C, and AA, BB and CC. Matrices A and B contain off-diagonal elements of the matrix A, and matrix C contains diagonal elements of A. Note that A=B. Similarly, AA and BB contain off-diagonal elements of the matrix B, while in CC its diagonal elements are stored. Again AA=BB. The program was written assuming

that A=B and AA=BB but it should not be any problem with its generalization.

Elements of the matrix C are calculated in the subroutine CTAB using output from the subroutine FLUCT. If the model assumes no changes of the electron density in the z direction, matrices C and CC can be calculated outside the loop DO 2 J=1,N.

Subroutine MOZAX performs the matrix multiplication. It multiplies the matrix A by the matrix Y which contains the complex amplitude at the preceding level or the initial values.

Subroutine PROGON solves the system of equations using the Thomas algorithm described in Section 4.

```
      PROGRAM SMEET(INPUT,OUTPUT,TAPE4=ELF,TAPE5=RESULT,PASS,DA2,TAPE1=RESULT,
     *TAPE2=ELF,TAPE3=DA2,TAPE6=TERM,TAPE9=PASS)
C*****THIS PROGRAM IS USED TO SOLVE THE TWO-DIMENSIONAL PARABOLIC EQUATION
C     FOR A DIVE PROPAGATING IN THE IRREGULAR IONOSPHERE OR IN A FREE SPACE
C     AFTER PASSING THROUGH A PHASE CHANGING SCREEN. THE METHOD DESCRIBED IN THE
C     REPORT IS USED.
C*****
C*****THE MODEL OF IRREGULARITIES IS CALCULATED IN THE SUBROUTINE FLUCT.SUB-
C     ROUTINE VDIS IS USED TO SET THE INITIAL VALUES FOR A PHASE SCREEN.THEY
C     ARE CALCULATED IN THE SUBROUTINE VDIS.SUBROUTINE GIAR CALCULATES THE E-
C     XPANSION OF THE MATRIX C.SUBROUTINE MOLAX IS USED TO CALCULATE THE PRO-
C     DUCT OF TWO MATRICES.AND THE SUBROUTINE PROCON TO SOLVE THE SYSTEM
C     OF EQUATIONS ACVOP.
C*****
C*****THE FILES PERFORM THE FOLLOWING FUNCTIONS:
C     RESULT-CONTAINS THE HIGH-ACCURACY RESULTS OF COMPUTATIONS.AFTER RE-
C     NAMING TO PASS THIS FILE CAN BE USED FOR FURTHER CALCULATIONS.FOR
C     INSTANCE,WITH THE CHANGED STEP-SIZE OR OUTSIDE THE IRREGULAR MEDIUM.
C     ELF-CONTAINS INFORMATIONS ABOUT THE HORIZONTAL IRREGULAR STRUCTURE.
C     TERM-IS USED FOR SUBSEQUENT PRINTING OF RESULTS WITH REDUCED ACCURACY
C     AND ONLY FOR CHOSEN MACH POINTS.
C     DA2-CONTAINS INPUT PARAMETERS
C*****
C*****INPUT PARAMETERS:
C     K-NUMBER OF STEPS IN THE HORIZONTAL X DIRECTION
C     N-NUMBER OF STEPS IN THE VERTICAL Z DIRECTION
C     H-STEP SIZE IN THE Z DIRECTION (M
C     DU-STEP SIZE IN THE X DIRECTION IN M
C     ALAM-WAVELENGTH,FACTOR(SEE REPORT)
C     FREQ-THE CHOSEN FREQUENCY IN MHZ
C     N1- N1=0 FOR THE PHASE SCREEN
C     KSKIP-NUMBER OF STEPS IN THE X DIRECTION RECORDED ON THE FILE PASS
C       (RENAMED FILE RESULT) OVER WHICH ONE HAVE TO SKIP TO FIND THE INI-
C       TIAL VALUES FOR FURTHER COMPUTATIONS IF IT MAY HAVE STOPED FOR ANY
C       REASON.FOR INSTANCE,TRANSITION FROM COMPUTATIONS INSIDE THE MEDIUM
C       TO THOSE OUTSIDE THE MEDIUM)
C     KM-ONLY EVERY KM STEP IN THE X DIRECTION IS RECORDED ON FILES RESULT
C     AND TERM
C     KK-ONLY EVERY KK STEP IN THE Z DIRECTION IS RECORDED ON THE FILE TERM
C     IC= IC=1 FOR COMPUTATIONS INSIDE THE IRREGULAR MEDIUM,IC=0 OUTSIDE
C     THE MEDIUM AND FOR THE PHASE SCREEN
C     KL-NUMBER OF STEPS IN THE Z DIRECTION COMPUTED IN THE PREVIOUS RUNS
C       (USED TO CALCULATE A DISTANCE FROM Z=0 TO THE ACTUAL LEVEL)
C     MP-IF MP=0 NO LEADING INDICATOR OF APS INPUT VALUES RECORDED ON
C     THE FILE PASS ARE READ,OTHERWISE IT IS ASSUMED THAT THEY WERE NOT
C     RECORDED
C     M2- IF M2=0 THE INPUT FILE ELF1 IS READ. IT DOES NOT NEED TO BE READ
C       FOR CALCULATION OUTSIDE THE IRREGULAR MEDIUM
C     REMARK: THE REST OF PARAMETERS APPLY ONLY TO THE IRREGULARITY MODEL
C     DESCRIBED IN THE REPORT.
C     AL,BE1,BE2 ARE USED TO CALCULATE THE WEIGHTING FUNCTION,
C     THEY ARE ALSO USED TO CALCULATE THE PARABOLIC REFRACTION CONCENTRA-
C     TION PROFILE, WHICH IS THE ASSUMED RMS PHASE ON THE PHASE SCREEN
C*****
```

THIS PAGE IS BEST QUALITY PRACTICABLE
FROM COPY FURNISHED TO DDC

```
      COMMON/PLU/ELX(888),PHI0
      COMMON/CI/IC,FREQ,N,NTAU,PI,PP,RKI
      COMMON/DA/ALP,BET,ZO,ZOO,ZMAX,EZ,ZMAX
      DIMENSION A(2,888),C(2,888),V(2,888),ALP(2,888),BT(2,888)
     *,R(2,888),F(888)
C     READ THE INPUT PARAMETERS
      DIMENSION AA(2,888),CC(2,888),AMP(888),PHI(888)
      READ(5,200)KK,TAU,A,SIGM,FREQ,N1,KSKIP
      READ(5,201)KK,KK,IC,ALP,PP,EZ
      READ(5,202)ALP,BET,ZOO,ZMAX,EZ,ZMAX,PHI0
  201 FORMAT(2I10,3F10.2,2I5)
  202 FORMAT(8E10.2)
  200 FORMAT(10A4,I1,A4,8(1X,F12.6),1X,2I6)
      TYPE 100,KK,TAU,A,SIGM,FREQ,N1,KSKIP
      TYPE 202,ALP,BET,ZOO,ZMAX,EZ,ZMAX,PHI0
  100 FORMAT(1H1,10A4,I1,A4/1H ,'KK=',F12.6,'  TAU=',F12.6,'  A=',F12.6
     *,'  SIGM=',F12.6/1H ,'FREQ=',F12.6,'  N1=',F12.6,'  KSKIP=',I6)
C     READ TAPE FILE ELX
      READ(2,311)(ELX(I),I=1,K)
  311 FORMAT(10E8.2)
   15 WRITE(3,203)ALP,BET,ZO,ZOO,ZMAX,EZ,ZMAX,PHI0
  203 FORMAT(1X,3HALP=,F10.2,2HKA=,2X,3HBET=,F10.2,2HKA=,2X,3HZO=,F10.2,2HKM,
     *2X,4HZOO=,F10.2,2HKA/1X,5HZMAX=,F10.2,6H/CA=3.,2X,5HEZ=,E10.2,
     *6H/CA=3.,2X,5HZMAX=,F10.2,2HKM/1X,5HPHI0=,F10.2)
      IF(KSKIP.NE.0)GO TO 275
      WRITE(3,273)K,N,TAU,A,SIGM,FREQ,N1,KSKIP
  273 FORMAT(2HK=,I4,2X,2HN=,I5,2X,4HTAU=,F11.8,2X,2HA=,F11.8,2X,
     *5HSIGM=,F9.6,2X,5HFREQ=,F8.3,2X,3HN1=,I5,2X,6HKSKIP=,I5)
C     IC=1 FOR WAVE INSIDE THE MEDIUM,IC=0 FOR WAVE OUTSIDE THE MEDIUM
  275 PI=4.*ATAN(1.)
C     NORMALIZE THE STEP SIZE TO THE WAVE NUMBER
      RKI=300./(2.*PI*FREQ)
      TAU=TAU/RKI
      H=H/RKI
      PP=60.0E-6/(FREQ*FREQ)
C     SET INITIAL VALUES TO THE V MATRIX.V(1,N)=RE PART OF V,V(2,N)=IM
C     PART OF V.IF THE PHASE SCREEN CALL VOI.IF KSKIP.NE.0 READ THE FILE PASS
      IF(N.EQ.1)GO TO 1200
      IF(KSKIP)1200,1200,1220
 1200 CALL VO(V,K)
      GO TO 1
 1220 CALL VO1(V,K)
      GO TO 1
 1228 IF(NP.)1240,1240,1230
 1230 READ(5,236)A1,A2,A3,A4,A5,A6,A7,A8
      PRINT 236,A1,A2,A3,A4,A5,A6,A7,A8
 1240 DO 1230 I=1,NSKIP
      READ(5,233)T1,B1,T2,T3,IC1
      READ(5,233)(V(1,I),V(2,I),AMP(I),PHI(I),I=1,K)
      PRINT 300,I
      PRINT 233,T1,B1,T2,T3,IC1
 1230 CONTINUE
    1 CONTINUE
C     SET VALUES TO A AND AA MATRICES.
      DO 1 I=1,K
      A(1,I)=0.
      A(2,I)=-1./(H*H)
      AA(1,I)=0.
    1 AA(2,I)=ALP(2,I)*TAU*SIGM
C     SET VALUES ON THE DIAGONAL(C AND CC MATRICES) IF INSIDE THE MEDIUM FIRST
C     COMPUTE THE DIELECTRIC PERMITTIVITY FLUCTUATIONS AND THE FUNCTION P,THEN
C     CALL CTAB
      IF(IC.EQ.1)GO TO 28
      DO 8 I=1,K
      C(1,I)=0.
      C(2,I)=-1./(H*H)
    8 CC(1,I)=C(1,I)*TAU*SIGM
   28 CONTINUE
      DO 2 I=1,N
C     SET VALUES ON THE DIAGONAL(C AND CC MATRICES)
      IF(IC.EQ.0)GO TO 55
      CALL CTAB(P,C,K)
      CALL CTAB(P,C,K)
      DO 3 I=1,K
      CC(1,I)=C(1,I)*TAU*SIGM
    3 CC(2,I)=C(2,I)*TAU*SIGM
C     COMPUTE THE PRODUCT E=A*V
   55 CALL MOTRX(A,AA,C,V,E,K)
C     SOLVE THE EQUATION A*E=V WHERE A=TRIDIAGONAL MATRIX
      CALL PROCON(AA,A,CC,E,ALP,BT,K)
C     CALCULATE RE AND IM PARTS OF THE COMPLEX AMPLITUDE AND AMPLITUDE AND PHASE
      DO 4 I=1,K
      V(1,I)=V(1,I)-TAU*E(1,I)
      V(2,I)=V(2,I)-TAU*E(2,I)
      PHI(I)=ATAN2(V(2,I),V(1,I))
      AMP(I)=SQRT(V(1,I)*V(1,I)+V(2,I)*V(2,I))
      IF(PHI(I).GT.PHI(I)+2.*PI*PHI(I))
      PHI(I)=PHI(I)/PI
```

THIS PAGE IS BEST QUALITY PRACTICABLE
FROM COPY FURNISHED TO DDC

```
    4 CONTINUE
      B(J)=(J-1)*TAU*0.5D0/(2.*PI*FREQ)
  555 RR(J)=ZR
      RR=ZR
      IF(J.EQ.N)GO TO 9
      IF(ZR.NE.RR)GO TO 8
    9 WRITE(6,333)(I,I=1,IC
      WRITE(6,333)(V(I,I),V(2,I),AMP(I),PHI(I),I=1,R,RR)
      WRITE(1,333)(V(I,I),V(2,I),AMP(I),PHI(I),I=1,R)
    8 CONTINUE
  222 FORMAT(1H ,F10.4,2E12.4)
  444 FORMAT(1H0,'DISTANCE=',F10.4,3X,'HKM',3X,'HICO=',I4,3X)
  333 FORMAT(1H ,F10.4,A2,3I3,I4,3I)
  334 FORMAT(1H ,5X,4(I6,I8))
  230 FORMAT(46,2I,A1,2I,A1,I5,2X,A13,2X,A11,2X,A13,2X,A8,2X,A11)
      ENDFILE 1
   10 CONTINUE
  300 FORMAT(1X,'SKIP=',I6)
      STOP
      END
      SUBROUTINE TOI(V,L)
C     THIS SUBROUTINE SETS THE INITIAL VALUES TO THE MATRIX V
      DIMENSION V(2,L)
      DO 1 I=1,L
      V(1,I)=0.0
    1 V(2,I)=0.0
      RETURN
      END
      SUBROUTINE FLUCT(F,J,R)
C     THIS SUBROUTINE CALCULATES THE DIELECTRIC PERMITIVITY AND THE F FUNCTION
C     FOR A GIVEN MODEL OF THE IONOSPHERIC ELECTRON DENSITY FLUCTUATIONS,
C     MODEL OF THE BACKGROUND DENSITY AND THE WEIGHTING FUNCTION G.
      COMMON/FLU/ELK(1000),EM,G
      COMMON/CT/IC,PHI,M,N,IV,PI,FP,ERI
      COMMON/ON/DEL,ZO,ZOO,CMAX,EI,ZMAX
      DIMENSION V(2,1)
      ZR=V(1,J)=R*ERI
      ZI=V(2,J)=ZR
      IF(Z.LE.ZO)GO TO 30
      IF(Z.GT.ZOO)GO TO 40
      G=1.0
      GO TO 50
   30 ARG=((Z-ZO)/DEL)**2
      IF(ARG.GT.660.)GO TO 31
      G=EXP(-ARG)
      GO TO 32
   31 G=0.0
   32 ARG=((ZI-ZO)/DEL)**2
      IF(ARG.GT.660.)GO TO 33
      G=EXP(-ARG)
      GO TO 50
   33 G=0.0
      GO TO 50
   40 ARG=((Z-ZOO)/DEL)**2
      IF(ARG.GT.660.)GO TO 41
      G=EXP(-ARG)
      GO TO 42
   41 G=0.0
   42 ARG=((ZI-ZOO)/DEL)**2
      IF(ARG.GT.660.)GO TO 43
      G=EXP(-ARG)
      GO TO 50
   43 G=0.0
   50 HA=(MAX1/(ABS(1.-EI/EMAX)
      COEFF=(1.-((Z-ZMAX)/HH)**2)*G
      IF(EMAX.GT.1)GO TO 10
      COEFF=(1.-((ZI-ZMAX)/HH)**2)*G
      FACT=((E-1)*0.5
      GO TO 20
   10 FACT=0.0
   20 DO 1 I=1,M
      F(I)=COEFF*FACT*(ELK(I)/ELK(M)-1.)
    1 CONTINUE
      RETURN
      END
```

THIS PAGE IS BEST QUALITY PRACTICABLE
FROM COPY FURNISHED TO DDC

```
      SUBROUTINE CTAB(C,C,N)
      COMMON/[illegible]
      DIMENSION [illegible]
      [illegible]
      [illegible]
      [illegible]
      C[illegible]=1./(FLOAT(N)*C[illegible])
      RETURN
      END
      SUBROUTINE MODAB(A,B,C,Y,A,N)
      COMMON/[illegible]
C     SUBROUTINE TO CALCULATE THE PRODUCT A*Y=B, WHERE A,B,Y ARE
      COMPLEX A,B,Y,C,TEMP,FACTOR
CC    BE REMARK BE THE FACT THAT A=B IS USED IN THE SUBROUTINE
      DIMENSION A(2,N),B(2,N),C(2,N),Y(2,N),X(2,N)
      M=N-1
      DO 100 I=2,M
      X(1,I)=A(1,I-1)*Y(1,I-1)+A(2,I-1)*Y(2,I-1)+C(1,I)*Y(1,I)+C(2,I)*
     *Y(2,I)+B(1,I)*Y(1,I+1)+B(2,I)*Y(2,I+1)
      X(2,I)=A(1,I-1)*Y(2,I-1)+A(2,I-1)*Y(1,I-1)+C(1,I)*Y(2,I)+C(2,I)*
     *Y(1,I)+B(1,I)*Y(2,I+1)+B(2,I)*Y(1,I+1)
  100 CONTINUE
      X(1,1)=C(1,1)*Y(1,1)-C(2,1)*Y(2,1)+2.*(B(1,1)*Y(1,2)+
     *B(2,1)*Y(2,2))
      X(2,1)=C(2,1)*Y(2,1)+C(2,1)*Y(1,1)+2.*(B(1,1)*Y(2,2)+
     *B(2,1)*Y(1,2))
      X(1,N)=A(1,N-1)*Y(1,N-1)-A(2,N-1)*Y(2,N-1)+C(1,N)*Y(1,N)+
     *C(2,N)*Y(2,N)+0.5*(B(N)
      X(2,N)=A(1,N-1)*Y(2,N-1)+A(2,N-1)*Y(1,N-1)+C(1,N)*Y(2,N)+
     *C(2,N)*Y(1,N)+0.5*(B(N)
      RETURN
      END
      SUBROUTINE PROBON(A,B,C,Y,F,ALP,BT,N)
      DIMENSION A(2,N),B(2,N),C(2,N),Y(2,N),F(2,N)
      DIMENSION ALP(2,N),BT(2,N)
CCCCCC
C     SUBROUTINE SOLVES THE SYSTEM A*Y=F(A,Y,F=COMPLEX,A=TRIDIAGONAL)
C     USING THE THOMAS ALGORITHM.
C     LET'S CONSIDER THE SYSTEM
C           (1)  A(I)*Y(I-1)+C(I)*Y(I)+B(I)*Y(I+1)=F(I)  FOR N=2,3,...,N-1
C           (2)  Y(1)=-B(1)/C(1)*Y(2)+F(1)/C(1)
C           (3)  Y(N)=-A(N)/C(N)*Y(N-1)+F(N)/C(N)
C     ASSUME THE SOLUTION IS THE FORM
C           (4)  Y(I)=ALP(I+1)*Y(I+1)+BT(I+1)
C     WHERE
      ALP(2)=-B(1)/C(1)
      BT(2)=F(1)/C(1)
      DO 200 I=2,N-1
      ALP(I+1)=-B(I)/(A(I)*ALP(I)+C(I))
      BT(I+1)=(F(I)-A(I)*BT(I))/(A(I)*ALP(I)+C(I))
  200 CONTINUE
CCCCCC
C     BE REMARK BE THE FACT THAT A=B IS USED IN THE SUBROUTINE
      CNOR=C(1,1)**2+C(2,1)**2
      ALP(1,2)=-(B(1,1)*C(1,1)+B(2,1)*C(2,1))*2.0/CNOR
      ALP(2,2)=(B(1,1)*C(2,1)-B(2,1)*C(1,1))*2.0/CNOR
      BT(1,2)=(F(1,1)*C(1,1)+F(2,1)*C(2,1))/CNOR
      BT(2,2)=(F(1,1)*C(2,1)-F(2,1)*C(1,1))/CNOR
      M=N-1
      DO 100 I=2,M
      ROB1=C(1,I)*A(1,I-1)+ALP(1,I)-ALP(2,I)*A(2,I-1)
      ROB2=C(2,I)*A(1,I-1)+ALP(2,I)+ALP(1,I)*A(2,I-1)
      CNOR=ROB1**2+ROB2**2
      ALP(1,I+1)=-(B(1,I)*ROB1+B(2,I)*ROB2)/CNOR
      ALP(2,I+1)=(B(1,I)*ROB2-B(2,I)*ROB1)/CNOR
      ROB3=F(1,I)-A(1,I-1)*BT(1,I)+A(2,I-1)*BT
      ROB4=F(2,I)-A(1,I-1)*BT(2,I)-A(2,I-1)*BT
      BT(1,I+1)=(ROB3*ROB1+ROB4*ROB2)/CNOR
      BT(2,I+1)=-(ROB3*ROB2-ROB4*ROB1)/CNOR
  100 CONTINUE
      ROB1=C(1,N)*A(1,N-1)+ALP(1,N)*A(2,N-1)+ALP(2,N)
      ROB2=C(2,N)*A(1,N-1)+ALP(2,N)*A(2,N-1)+ALP(1,N)
      CNOR=ROB1**2+ROB2**2
      ROB3=F(1,N)-A(1,N-1)*BT(1,N)+A(2,N-1)*BT
      ROB4=F(2,N)-A(1,N-1)*BT(2,N)-A(2,N-1)*BT
      Y(1,N)=(ROB3*ROB1+ROB4*ROB2)/CNOR
      Y(2,N)=(ROB1*ROB4-ROB3*ROB2)/CNOR
      DO 101 I=1,M
      J=N-I
      Y(1,J)=ALP(1,J+1)*Y(1,J+1)-ALP(2,J+1)*Y(2,J+1)+BT(1,J+1)
      Y(2,J)=ALP(1,J+1)*Y(2,J+1)+ALP(2,J+1)*Y(1,J+1)+BT(2,J+1)
  101 CONTINUE
      RETURN
      END
      SUBROUTINE YDI(Y,E)
      COMMON/FLU/[illegible],PHIO
      DIMENSION Y(2,E)
      DO 1 I=1,E
      ELX=(I-1)*(X(E)-X(1))/(ELX(E)
      Y(1,I)=COS(ELX(I)*PHIO)
      Y(2,I)=SIN(ELX(I)*PHIO)
    1 CONTINUE
      RETURN
      END
```

THIS PAGE IS BEST QUALITY PRACTICABLE
FROM COPY FURNISHED TO DDC

```
      PROGRAM PLSC(INPUT,OUTPUT,RESULT,DA1,TAPE1=RESULT,TAPE2=DA1)
C*****************************************************************************
C     THIS PROGRAM IS USED TO PLOT THE DATA STORED ON THE FILE RESULT GENERA-
C     TED BY THE PROGRAM SHEET. PROGRAM USES THE GCS PACKAGE AND IS WRITTEN
C     FOR USE OF THE CALCOMP PLOTTER IF TEKTRONIX GRAPHICS TERMINAL IS
C     TO BE USED UDAREA MUST BE REFORMATTED AND CALL UPAUSE ADDED IN THE
C     PRINTOUT CALL UPAUSE AND REFORMATTED UDAREA ARE WRITTEN AS COMMENTS.
C     ON THE FILE RESULT USUALLY ARE STORED DATA COMPUTED AT SEVERAL LEVELS
C     EITHER INSIDE OR OUTSIDE THE SCATTERING MEDIUM. ANY CHOSEN LEVEL CAN
C     BE PLOTTED.
C*****************************************************************************
C*****************************************************************************
C     INPUT PARAMETERS:
C     NO-NUMBER OF LEVELS TO BE PLOTTED
C     N2-TOTAL NUMBER OF LEVELS STORED ON THE FILE RESULT
C     K-NUMBER OF POINTS IN THE X DIRECTION USED IN SHEET
C     K2-NUMBER OF POINTS IN THE X DIRECTION TO BE PLOTTED(K2.LE.K)
C     KSKIP-IF KSKIP=0 IT IS ASSUMED THAT THE SHEET PROGRAM INPUT PARAMETERS
C       ARE NOT WRITTEN ON THE FILE RESULT
C     M-THE STEP SIZE IN THE X DIRECTION USED IN THE PROGRAM SHEET (IN M)
C     M(J)-CONSECUTIVE NUMBER OF THE LEVEL ON THE FILE RESULT WHICH HAVE TO
C       BE PLOTTED.
C*****************************************************************************
      DIMENSION T1(800),T2(800),AMP(800),PHI(800),M(20),X(800)
      READ(2,100) NO,N2,K2,KSKIP,K,M
      READ(2,105)(M(J),J=1,NO)
      IF(KSKIP.EQ.0)GO TO 50
      READ(1,101)T1,K,T2,N,T3,TAU,T4,M,T5,SIGM,T6,FREQ,T7,N1,T8,KSKIP
   99 DO 1 I=1,K2
    1 X(I)=I*M/1000.
      CALL USTART
      DO 3 J=1,N2
      READ(1,103)A1,T1,A2,A3,IC
      READ(1,101)(T1(I),T2(I),AMP(I),PHI(I),I=1,K)
      DO 3 NN=1,NO
      IF(J.NE.M(NN))GO TO 3
      CALL UCREATE
      CALL UCHECK
      CALL USET('LINE')
      GO TO(10,20,30,40),IC
C  10 CALL UDAREA(0.00,10.00,3.00,7.3,10.0)
C  10 CALL UDAREA(1.75,4.00,4.2625,5.71)
      CALL USET('BOTH')
      CALL USET('XBOTH')
      CALL UPSET('YLABEL','RE U')
      CALL UPLOT(X,T1,FLOAT(K2))
      GO TO 3
C  20 CALL UDAREA(0.00,10.00,3.00,7.3)
C  20 CALL UDAREA(1.75,4.00,4.2625)
      CALL USET('BOTH')
      CALL UPSET('YLABEL','IM U')
      CALL UPLOT(X,T2,FLOAT(K2))
      GO TO 3
C  30 CALL UDAREA(0.00,10.0,2.5,3.0)
C  30 CALL UDAREA(1.75,7.00,1.4275,2.055)
      CALL USET('BOTH')
      CALL UPSET('YLABEL','AMPL')
      CALL UPLOT(X,AMP,FLOAT(K2))
      GO TO 3
C  40 CALL UDAREA(0.00,10.00,0.00,2.5)
C  40 CALL UDAREA(1.75,4.00,0.00,1.4275)
      CALL USET('BOTH')
      CALL USET('XBOTH')
      CALL UPSET('YLABEL','PHASE')
      CALL UPSET('XLABEL','DISTANCE(KM)')
      CALL UPLOT(X,PHI,FLOAT(K2))
C     CALL UPAUSE
C   2 CONTINUE
      CALL UFRSET
      CALL UCREATE
C     CALL UDAREA(0.00,10.00,0.0,10.0)
C     CALL UDAREA(1.75,4.00,0.0,5.71)
      CALL USET('BOTH')
      CALL USET('XBOTH')
      CALL UPSET('YLABEL','RE U')
      CALL UPSET('YLABEL','IM U')
      CALL UPSET('NUMBER')
      CALL UPSET('CHARACTER','*')
      CALL UPLOT(T1,T2,FLOAT(K2))
C   3 CONTINUE
      CALL UEND
  100 FORMAT(2I5,2F10.6)
  101 FORMAT(5E16.8)
  103 FORMAT(A10,I5,A5,I5,A3,I6,2X)
  104 FORMAT(A2,I4,2X,A2,I5,2X,A2,F11.4,2X,A2,F11.4,2X,A3,F6.4,2X,
     *A2,F8.4,2X,A5,I5,2X,A6,I5)
  105 FORMAT(8I16)
      STOP
      END
```

THIS PAGE IS BEST QUALITY PRACTICABLE
FROM COPY FURNISHED TO DDC

```
C*****THIS SUBROUTINE IS A STANDARD FAST FOURIER TRANSFORM. DURING COMPUTATION, THE
C INPUT ARRAY, DATA, IS DESTROYED AND REPLACED BY THE OUTPUT. THUS, DATA IS
C ALSO THE OUTPUT ARRAY.
C**********************************************************************
C
C**********************************************************************
C DATA IS THE INPUT ARRAY
C ISIGN = -1 MEANS TO TRANSFORM DATA
C ISIGN = +1 MEANS TO INVERSE TRANSFORM DATA.
C**********************************************************************
      SUBROUTINE FOURIER(DATA,NN,ISIGN)
      DIMENSION DATA(2048)
      N=2*NN
      J=1
      DO 7 I=1,N,2
      IF(I-J)1,2,2
    1 TEMPR=DATA(J)
      TEMPI=DATA(J+1)
      DATA(J)=DATA(I)
      DATA(J+1)=DATA(I+1)
      DATA(I)=TEMPR
      DATA(I+1)=TEMPI
    2 M=N/2
    3 IF(J-M)5,5,4
    4 J=J-M
      M=M/2
      IF(M-2)5,5,3
    5 J=J+M
      MMAX=2
    6 IF(MMAX-N)10,10
      ISTEP=2*MMAX
      ABSIGN=ISIGN
      AMAX=MMAX
      THETA=3.14159/(ABSIGN*AMAX)
      THETA2=2.*THETA
      SINTH=SIN(THETA)
      WSTPR=-2.*SINTH*SINTH
      WSTPI=SIN(THETA2)
      WR=1.
      WI=0.
      DO 9 M=1,MMAX,2
      DO 8 I=M,N,ISTEP
      J=I+MMAX
      TEMPR=WR*DATA(J)-WI*DATA(J+1)
      TEMPI=WR*DATA(J+1)+WI*DATA(J)
      DATA(J)=DATA(I)-TEMPR
      DATA(J+1)=DATA(I+1)-TEMPI
      DATA(I)=DATA(I)+TEMPR
    8 DATA(I+1)=DATA(I+1)+TEMPI
      TEMPR=WR
      WR=WR+WR*WSTPR-WI*WSTPI+WR
    9 WI=WI+WI*WSTPR+TEMPR*WSTPI+WI
      MMAX=ISTEP
      GO TO 6
   10 RETURN
      END
```

THIS PAGE IS BEST QUALITY PRACTICABLE
FROM COPY FURNISHED TO DDC

```
      PROGRAM SCINX(INPUT,OUTPUT,RESULT,DATA,TAPE1=DATA,TAPE2=RESULT)
      DIMENSION A1(600),AAP(600),V2(600),PHI(600),SCIN(10),NUM(10)
C*****THIS PROGRAM COMPUTES THE SCINTILLATION INDEX FOR
C     THE DATA STORED ON FILE RESULT.THE INPUT PARAMETERS ARE WRITTEN
C     ON THE FILE DATA.
C*****
C*****
C     INPUT PARAMETERS:
C     NSKIP-NUMBER OF LEVELS REGISTERED ON THE FILE RESULT TO BE SKIPED TO GET
C     TO THE DESIRED LEVEL.
C     K-NUMBER OF POINTS WRITTEN ON THE LEVEL
C     MO-NUMBER OF SEGMENTS OF THE DATA FOR WHICH SO MUST BE CALCULATED
C     NUM(J)-NUMBER OF POINTS IN EACH SEGMENT OF THE DATA
C*****
      READ(1,100)K,NSKIP,MO
      READ(1,101)(NUM(J),J=1,MO)
      PRINT 100,K,NSKIP,MO
      DO 1 I=1,NSKIP
      READ(1)
    1 CONTINUE
   20 PRINT 201,(I,I=1,K)
      DO 2 J=1,MO
      NSEG=K/NUM(J)
      DO 4 II=1,NSEG
      S1=0.0
      S2=0.0
      NI=NUM(J)*(II-1)+1
      NA=NUM(J)*II
      DO 3 I=NI,NA
      S2=AMP(I)**2+S2
    3 S1=AMP(I)+S1
      SCIN(II)=SQRT((S2/NUM(J))/((S1/NUM(J))**2)-1)
    4 CONTINUE
      PRINT 205,NUM(J)
      PRINT 204,(SCIN(II),II=1,NSEG)
    2 CONTINUE
  100 FORMAT(3I5)
  101 FORMAT(10I8)
  200 FORMAT(1X,F10.6,A2,3X,A3,I4,3X)
  201 FORMAT(3(5X,I5,5X))
  202 FORMAT(1X,2HAMPLITUDE=,F10.6,2HRM,3X,3HIC=,I4,3X)
  205 FORMAT(1X,4HNUM=,I5)
  204 FORMAT(1X,5(1X,F10.6))
      END
```

THIS PAGE IS BEST QUALITY PRACTICABLE
FROM COPY FURNISHED TO DDC

```
      PROGRAM RAND(ELPL,ELPL1,SPECTR,TAPE1=ELPL,TAPE2=ELPL1,TAPE3=
     *SPECTR)
      DIMENSION EL(2,1024),R(1024),PHI(1024),AMP(1024)
C*****THIS PROGRAM IS USED TO RANDOMIZE PHASES OF THE FOURIER TRANSFORMED DATA
C     IN INPUT DATA ARE STORED ON THE FILE ELPL PROPER CARE HAS TO BE TAKEN TO ASSURE
C     ZERO IMAGINARY PART OF THE OUTPUT DATA. REAL PART OF THE OUTPUT DATA AND
C     AMPLITUDE OF THE FOURIER COMPONENTS OF THE INPUT DATA ARE STORED ON
C     THE FILES ELPL1 AND SPECTR, RESPECTIVELY.
C     TO GENERATE RANDOM NUMBERS THE CYBER ROUTINE GGUBS IS USED,SUBROUTINE
C     FOUR PERFORMS FFT.
C*****
      DOUBLE DSEED
      DSEED=3.0D+4
      CALL GGUBS(DSEED,913,R)
      PI=4.*ATAN(1.)
      PI2=2.*PI
      READ(1,100)((EL(I,I),I=1,976)
      DO 1 I=1,1024
      IF(I.GT.976)GO TO 3
      EL(2,I)=EL(1,I)
      GO TO 4
    3 EL(1,I)=0.0
      EL(2,I)=0.0
    4 CONTINUE
    1 CONTINUE
      CALL FOUR(EL,1024,-1)
      DO 2 I=1,1024
      IF(I.EQ.1)GO TO 6
      AMP(I)=.5*ATAN2(EL(2,I),EL(1,I))+R(I)*PI2
      GO TO 7
    6 AMP(I)=.5*ATAN2(EL(2,I),EL(1,I))-R(1024-I)*PI2
    7 AMP(I)=SQRT((EL(2,I)*EL(2,I))+(EL(1,I)*EL(1,I)))
      EL(1,I)=AMP(I)*COS(AMP(I))
      EL(2,I)=AMP(I)*SIN(AMP(I))
    2 CONTINUE
      CALL FOUR(EL,1024,1)
      DO 9 I=1,976
      EL(1,I)=EL(1,I)/1024.
    9 CONTINUE
      WRITE(2,100)((EL(I,I),I=1,976)
      WRITE(3,101)(AMP(I),I=1,976)
  101 FORMAT(10F8.5)
  100 FORMAT(4(2X,F10.2))
      END
```

THIS PAGE IS BEST QUALITY PRACTICABLE
FROM COPY FURNISHED TO DDC

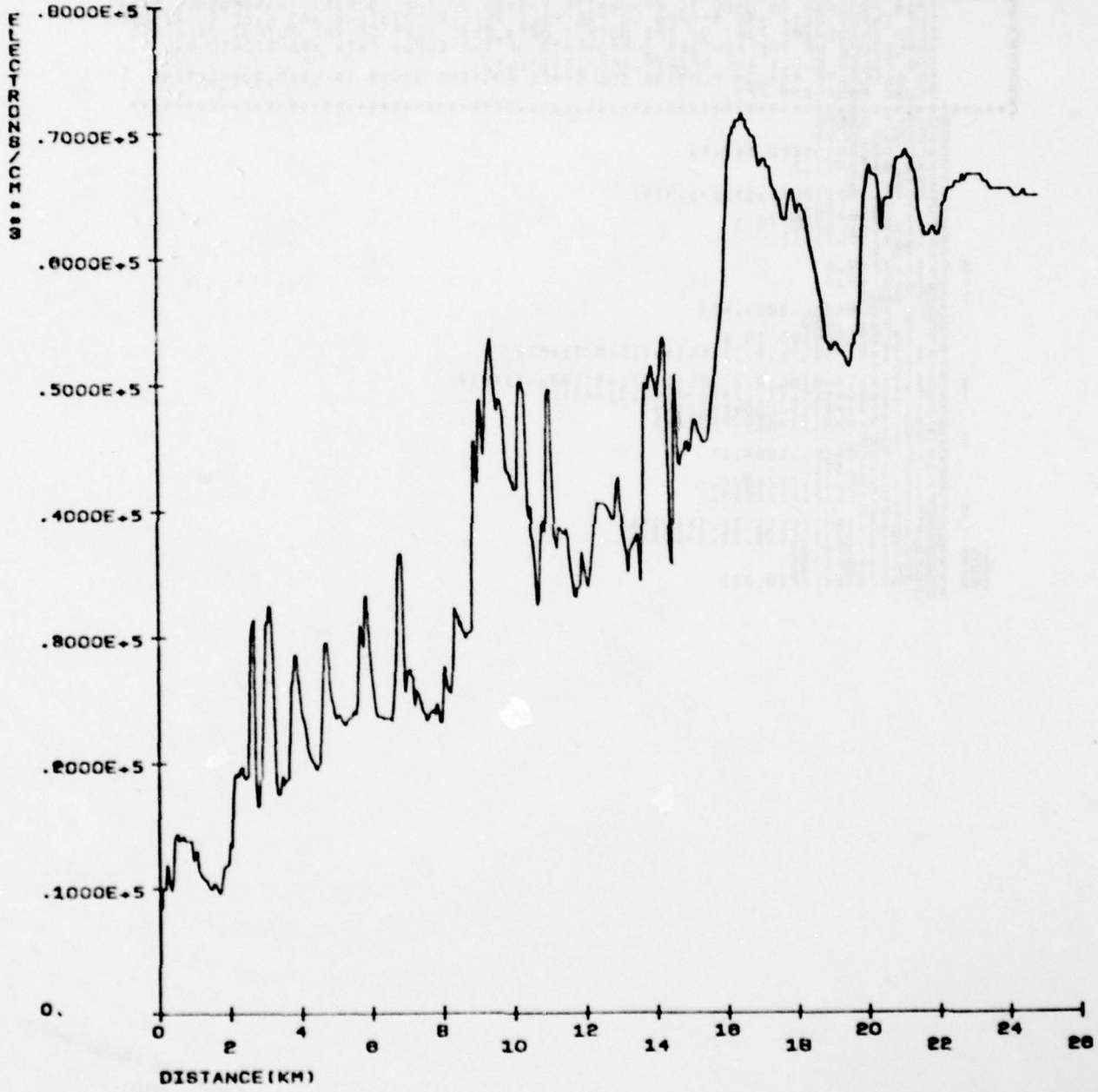


Fig. 1. High resolution electron density profile measured inside the plasma bubble. (Figure 7 of McClure et al. (1977) reconstructed after digitization.)

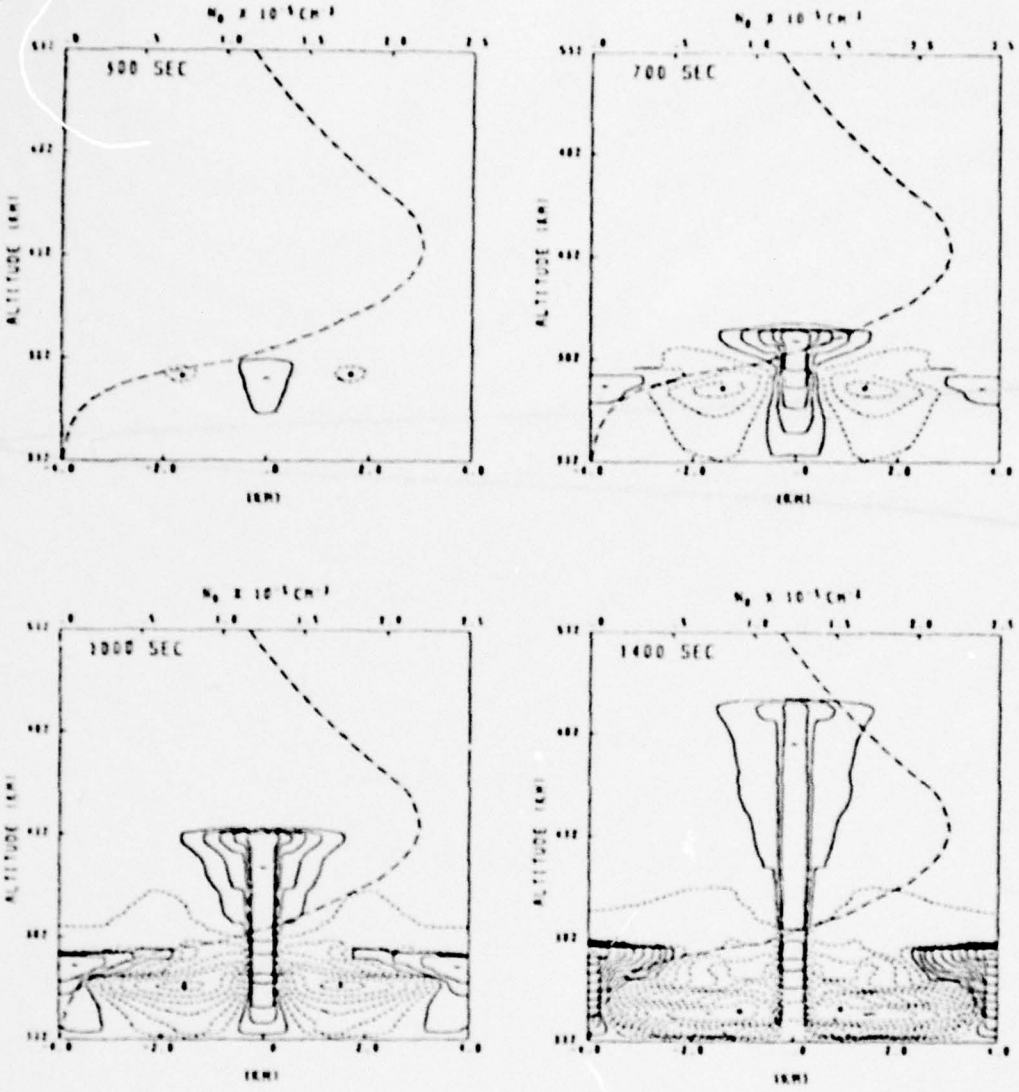


Fig. 2. Contour plots of constant $\Delta N/N$ at different stages of the bubble evolution as given by numerical simulation (Ossakow et al., 1979).

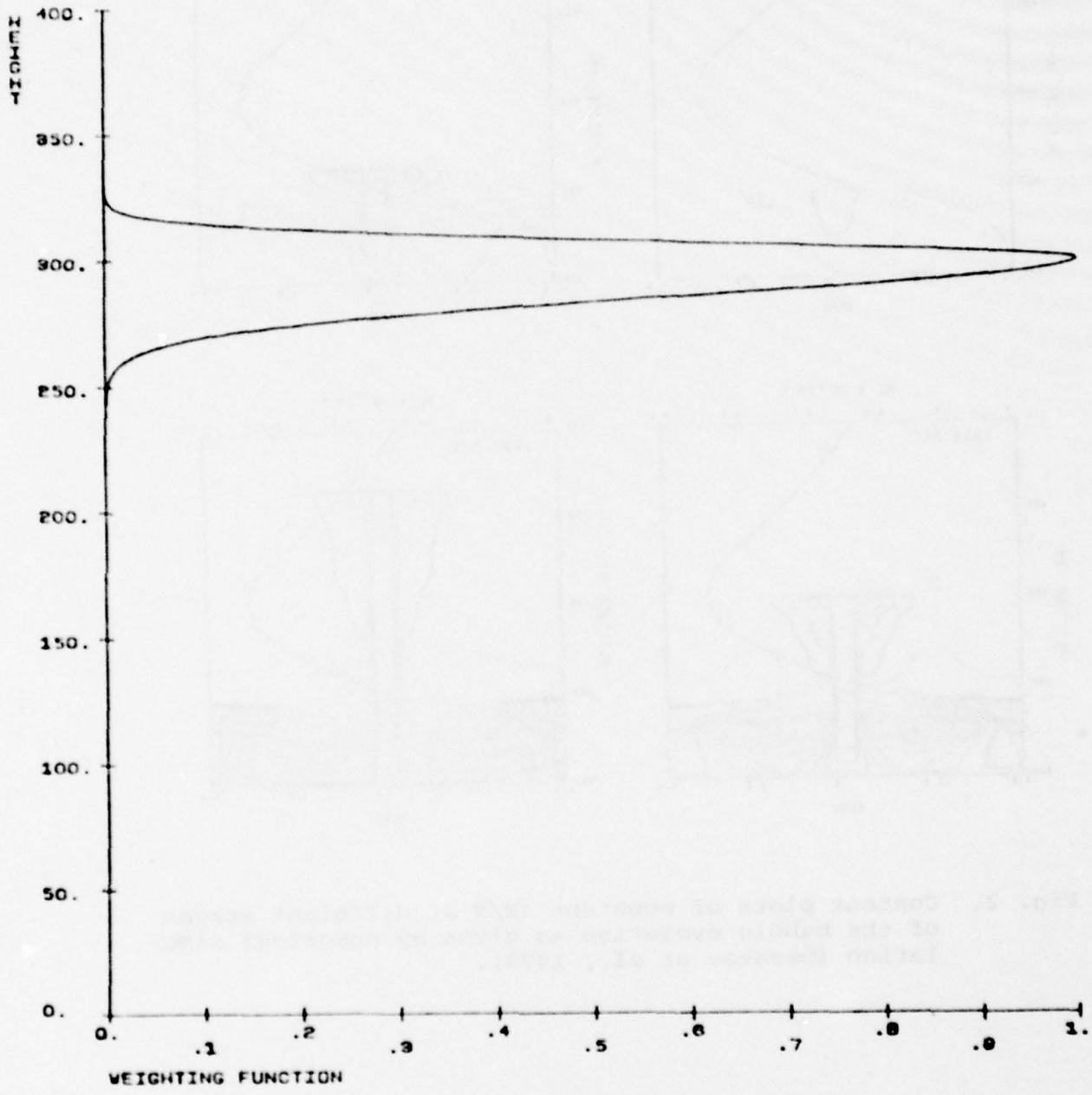


Fig. 3A. Weighting functions used to model "initial stage" of plasma bubble.

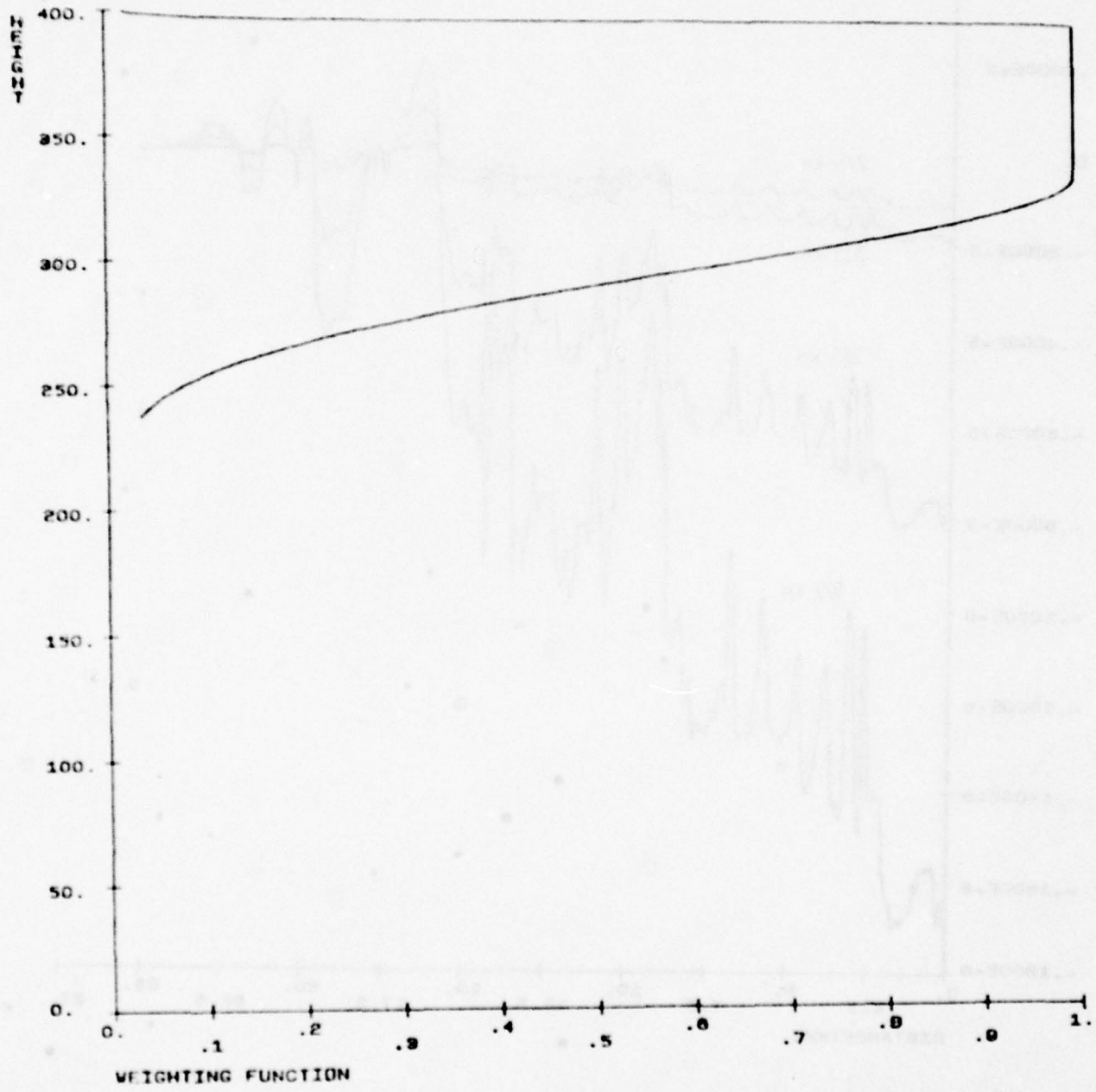


Fig. 3B. Weighting functions used to model "developed stage" of plasma bubble.

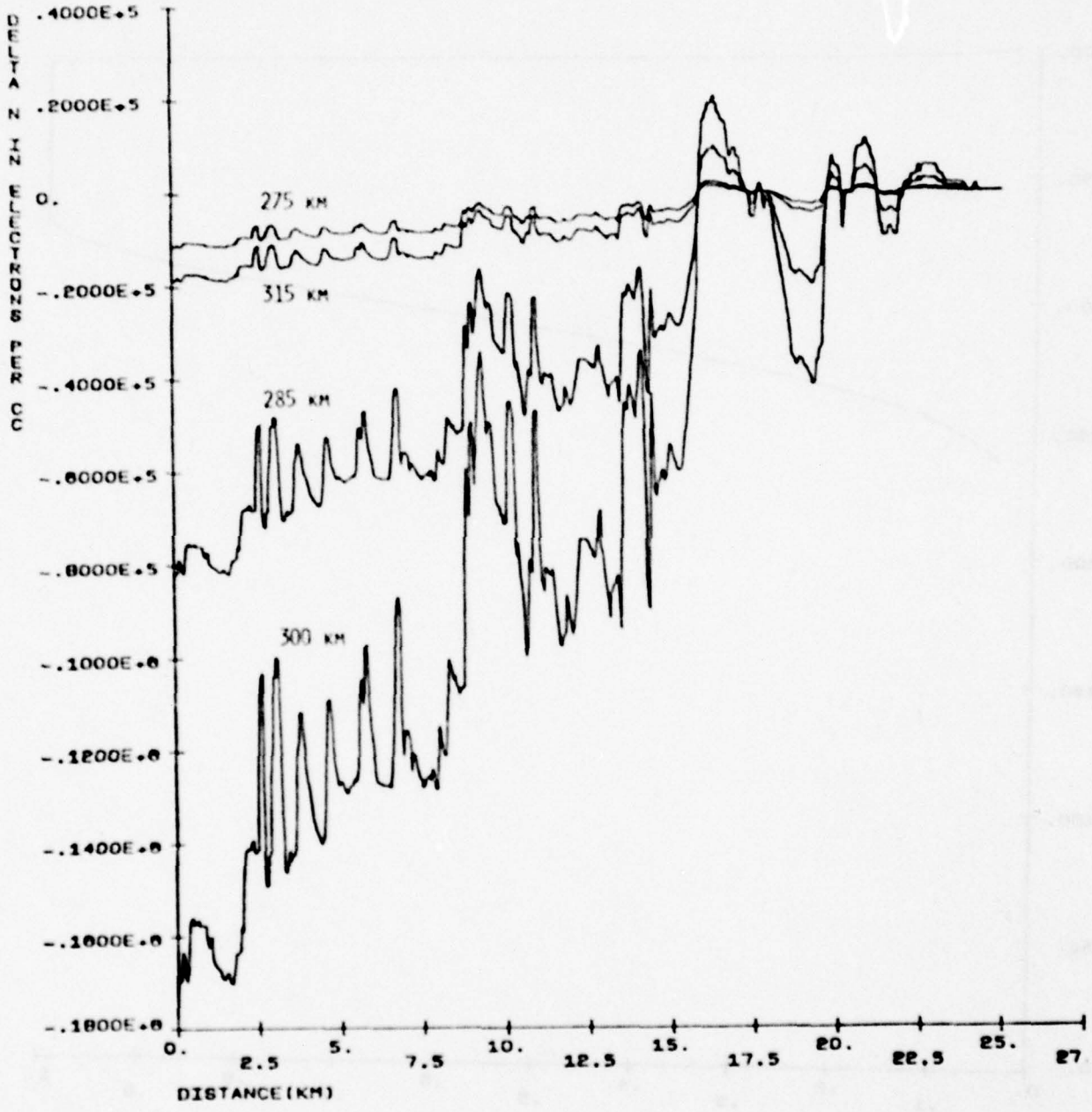


Fig. 4A. Horizontal electron density fluctuation profiles at different heights inside a plasma bubble, "initial stage."

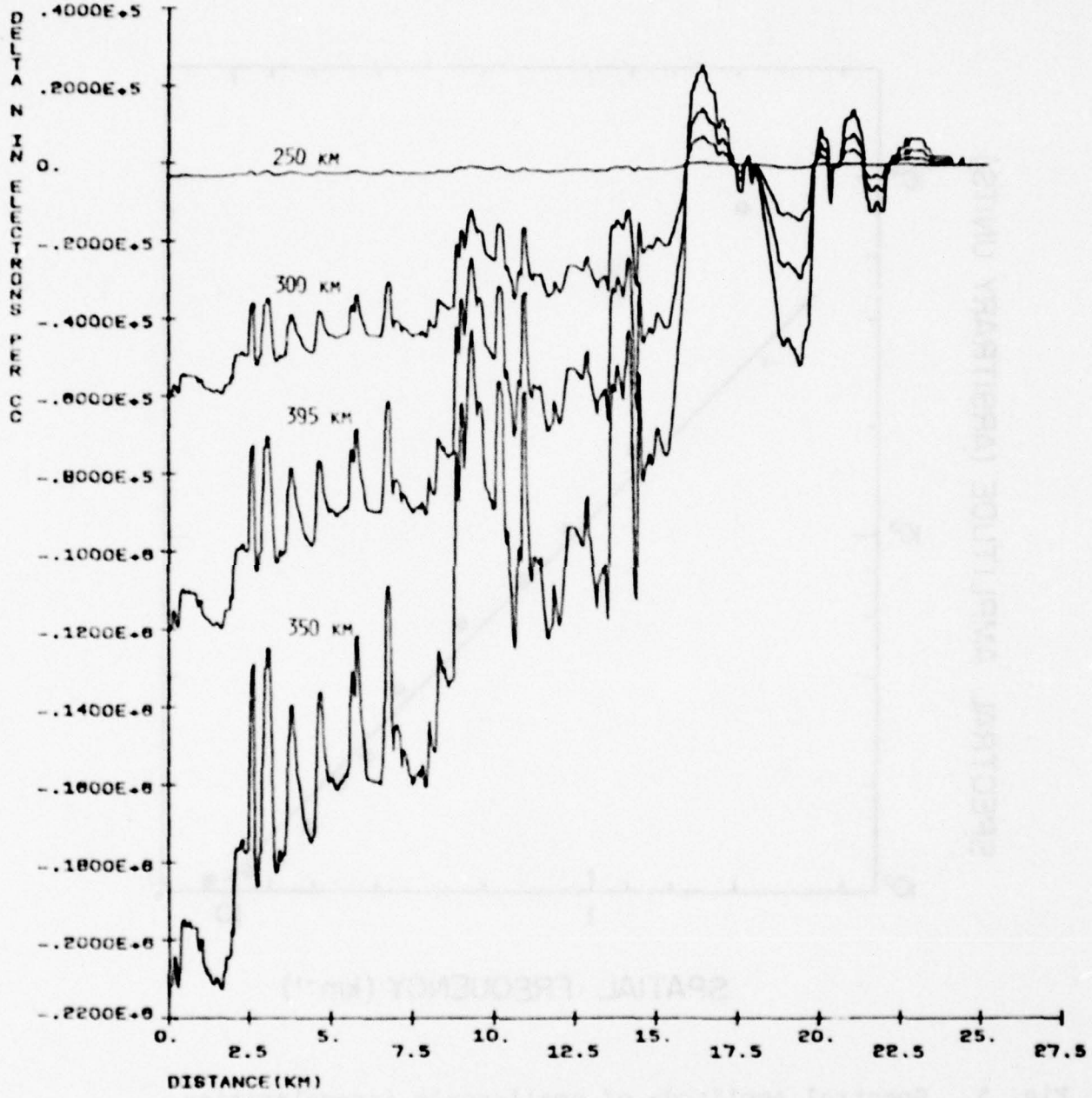


Fig. 4B. Horizontal electron density fluctuation profiles at different heights inside a plasma bubble, "developed stage."

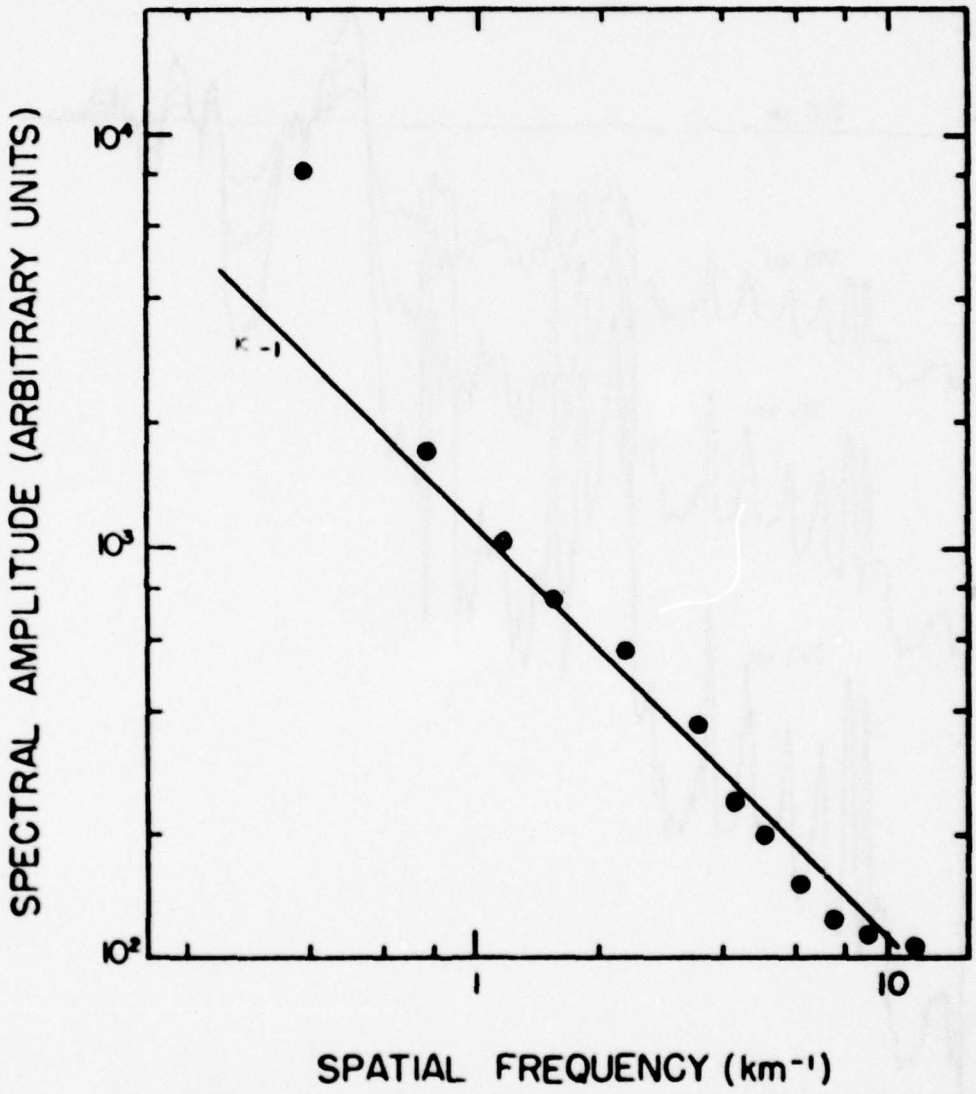


Fig. 5. Spectral amplitude of small-scale irregularities.

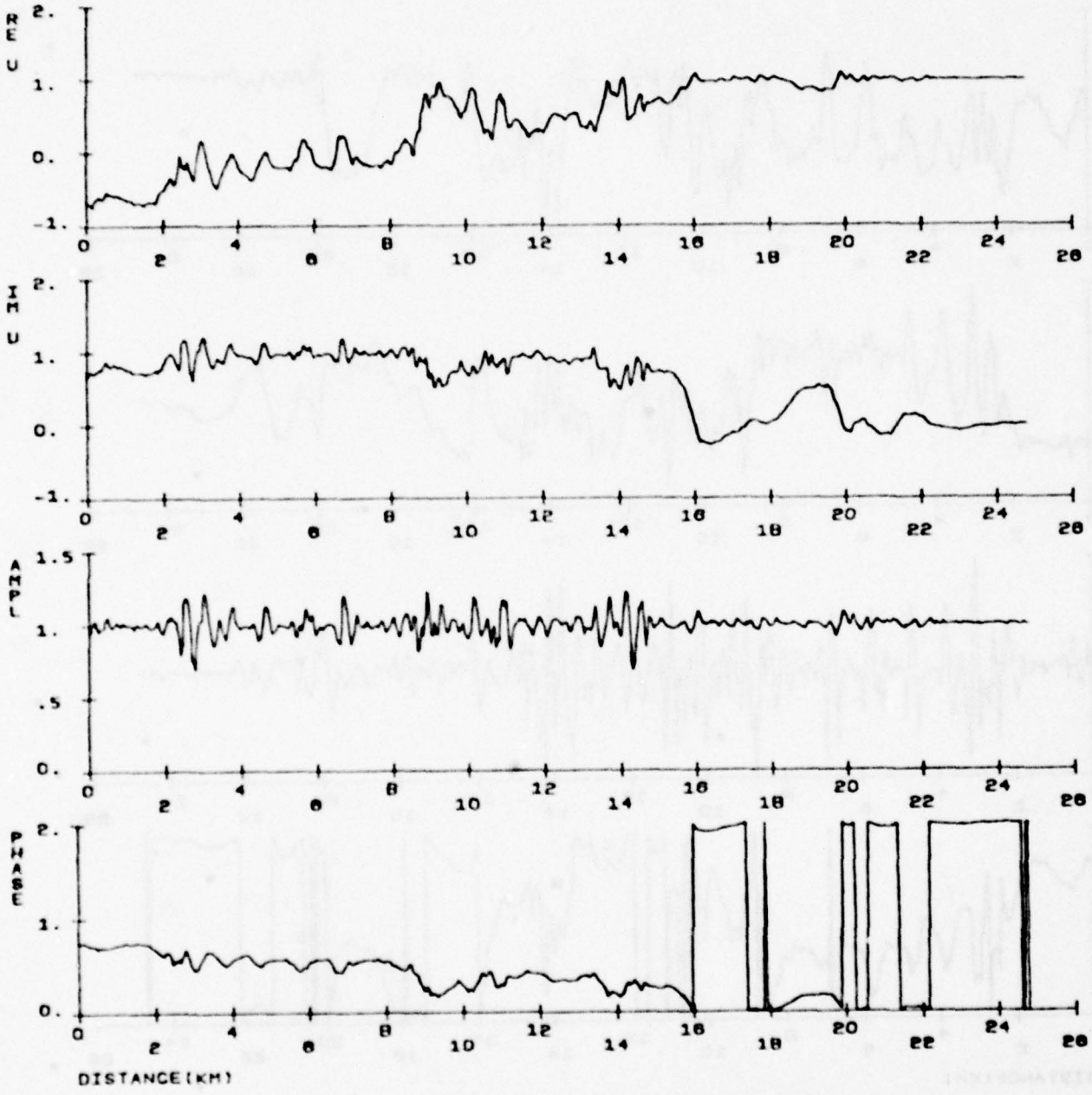


Fig. 6. Plots of the real and imaginary components of the complex amplitude, amplitude and phase (in π units) of a wave passing through the initial stage bubble and received on the ground. The wave frequency is 1500 MHz. Distance is measured from the projection of the center of the bubble on the ground.

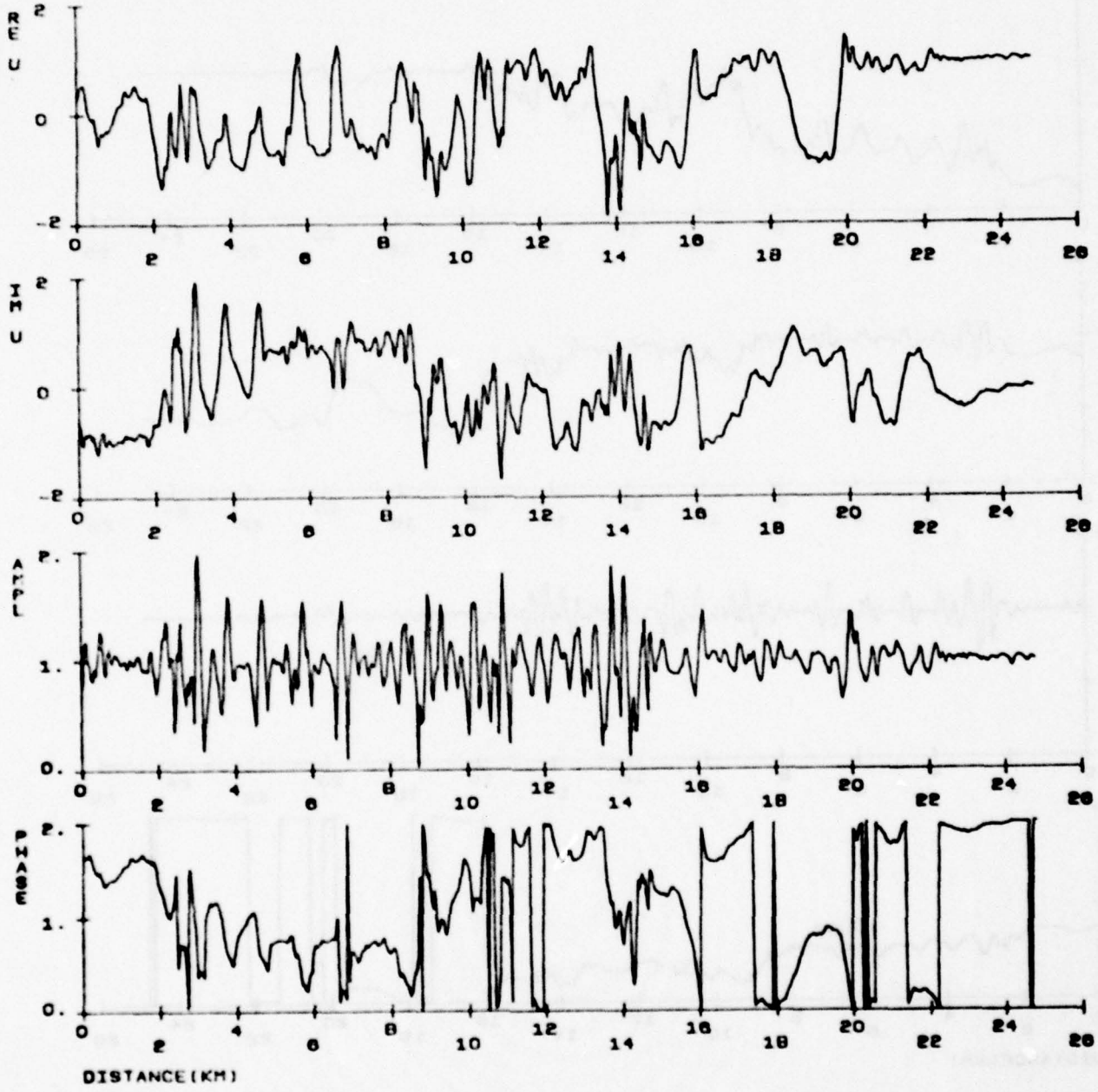


Fig. 7. Same as in Figure 6 but for the bubble in the developed stage.

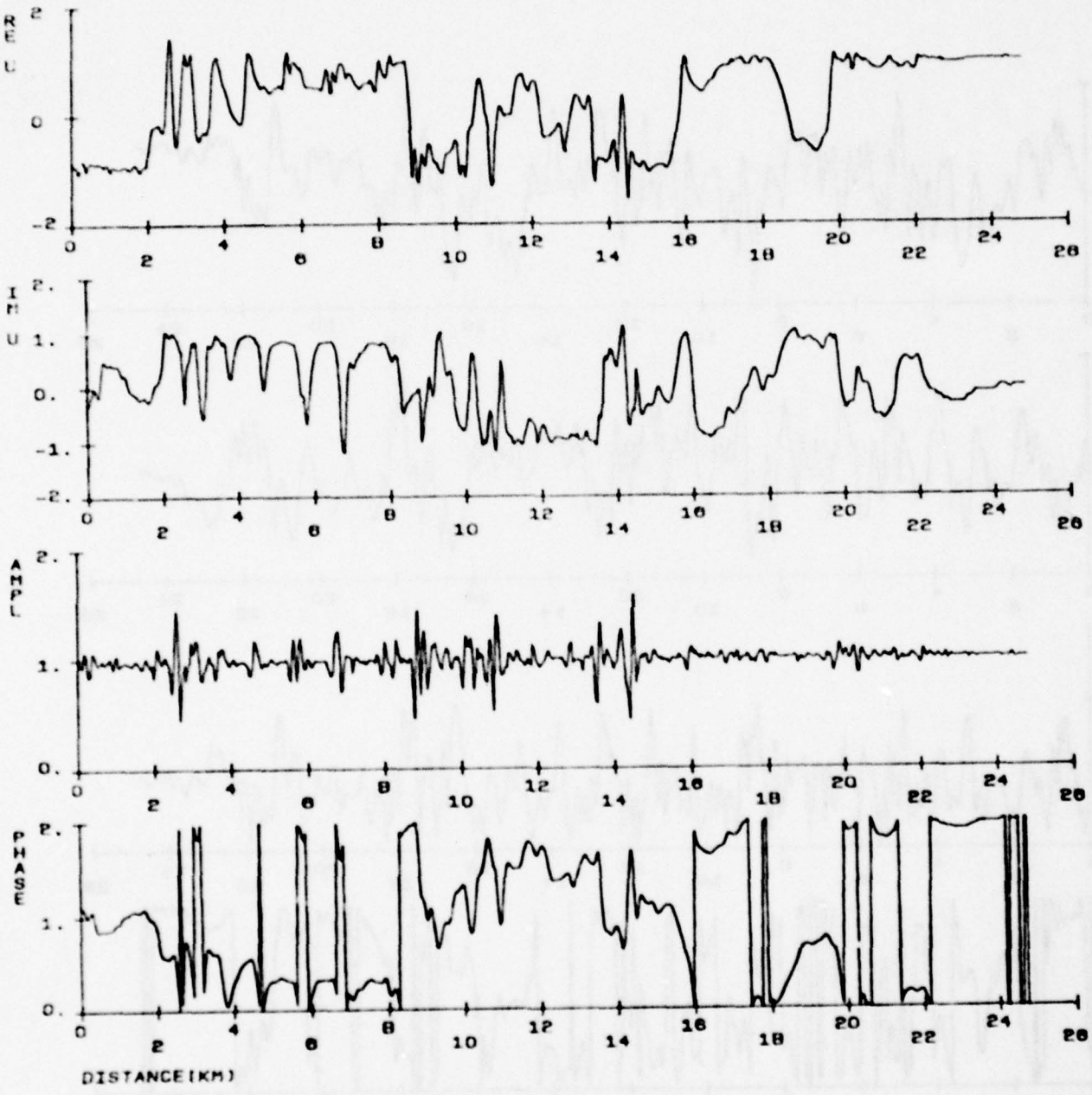


Fig. 8A. The same plots as in Figure 6 but at 136 MHz frequency. The wave structure at 300 km height is given.

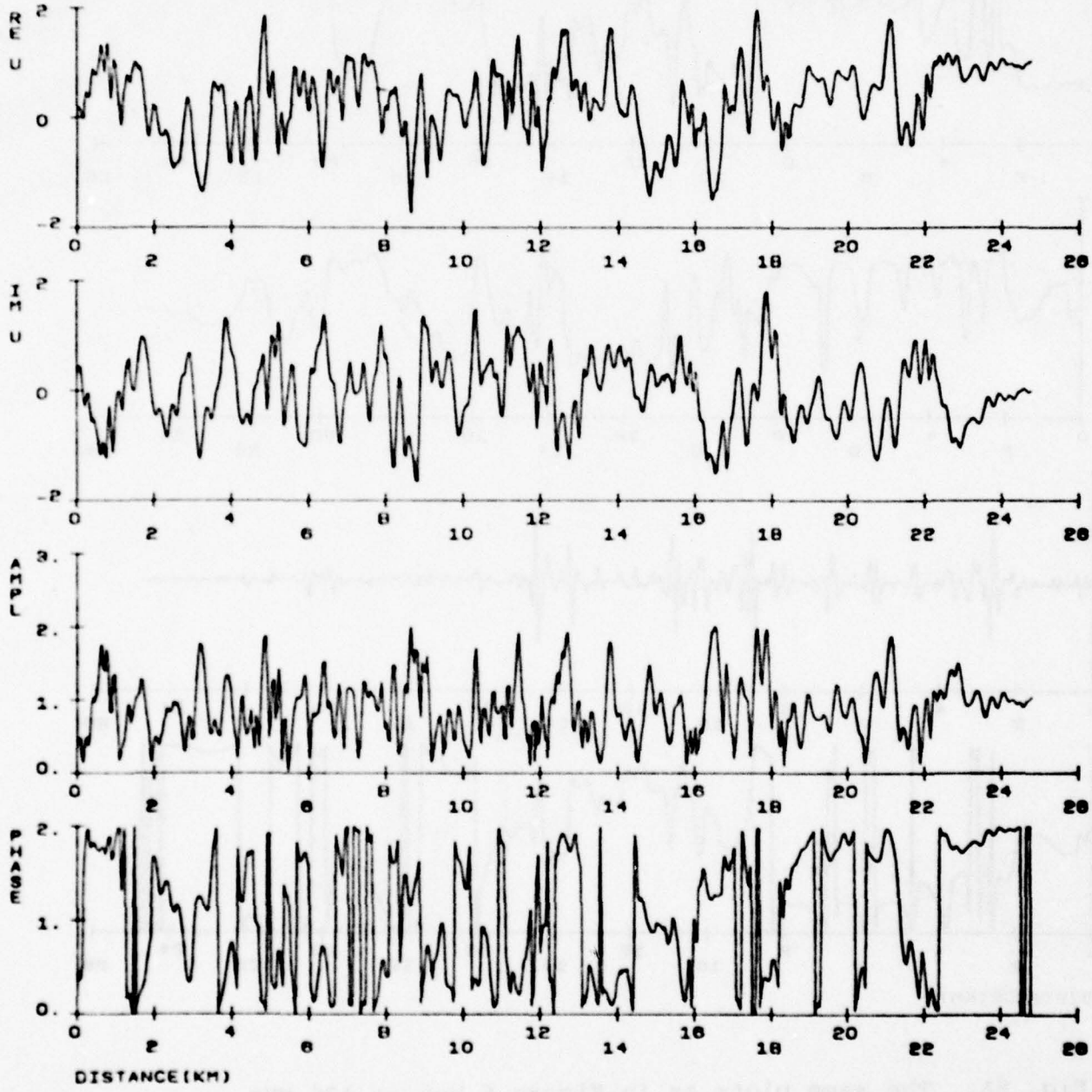


Fig. 8B. The same plots as in Figure 6 but at 136 MHz frequency. The wave structure on the ground is given.

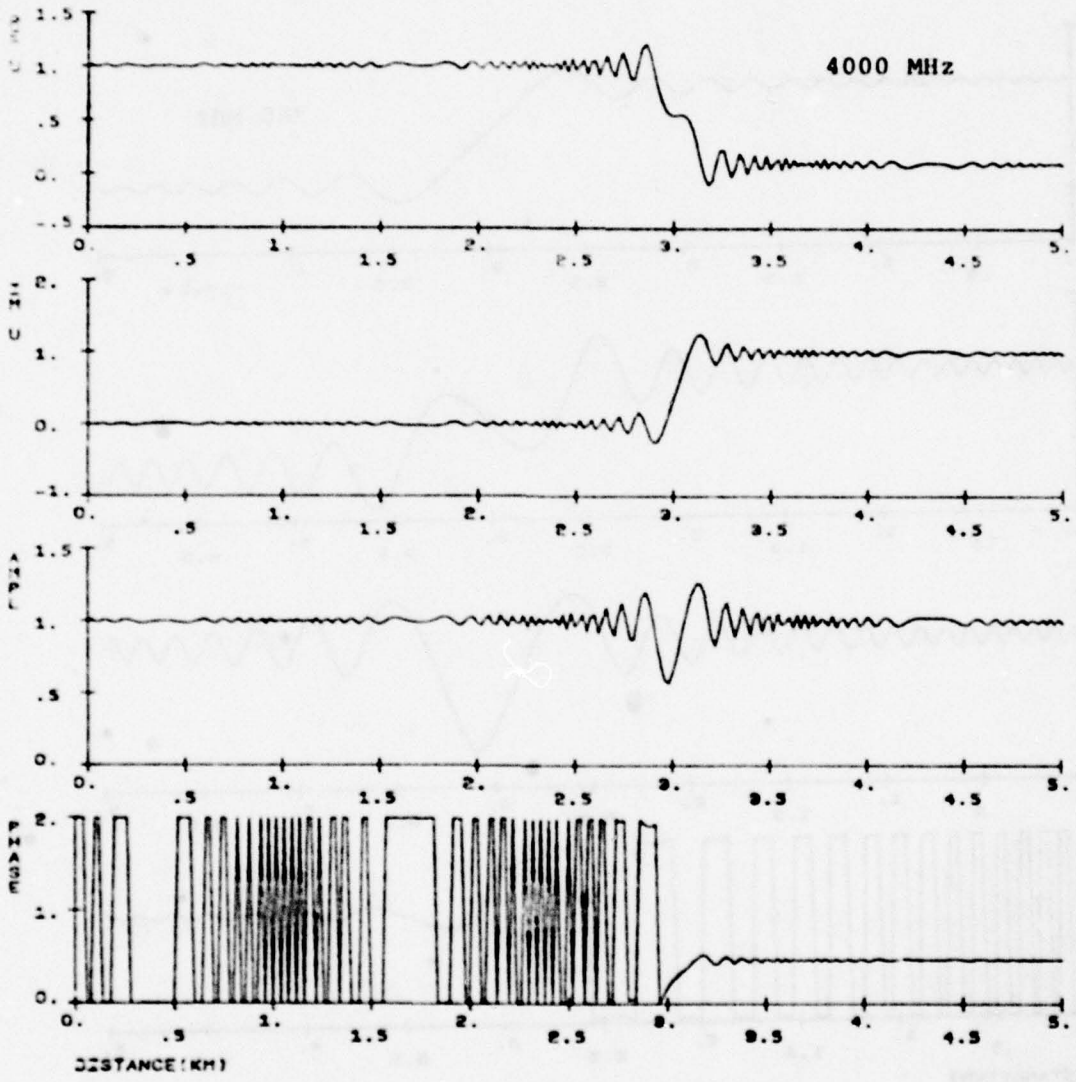


Fig. 9A. Wave structure after passing through a phase screen with discontinuity at a distance of 3 km. The phase screen height is 350 km at 4000 MHz.

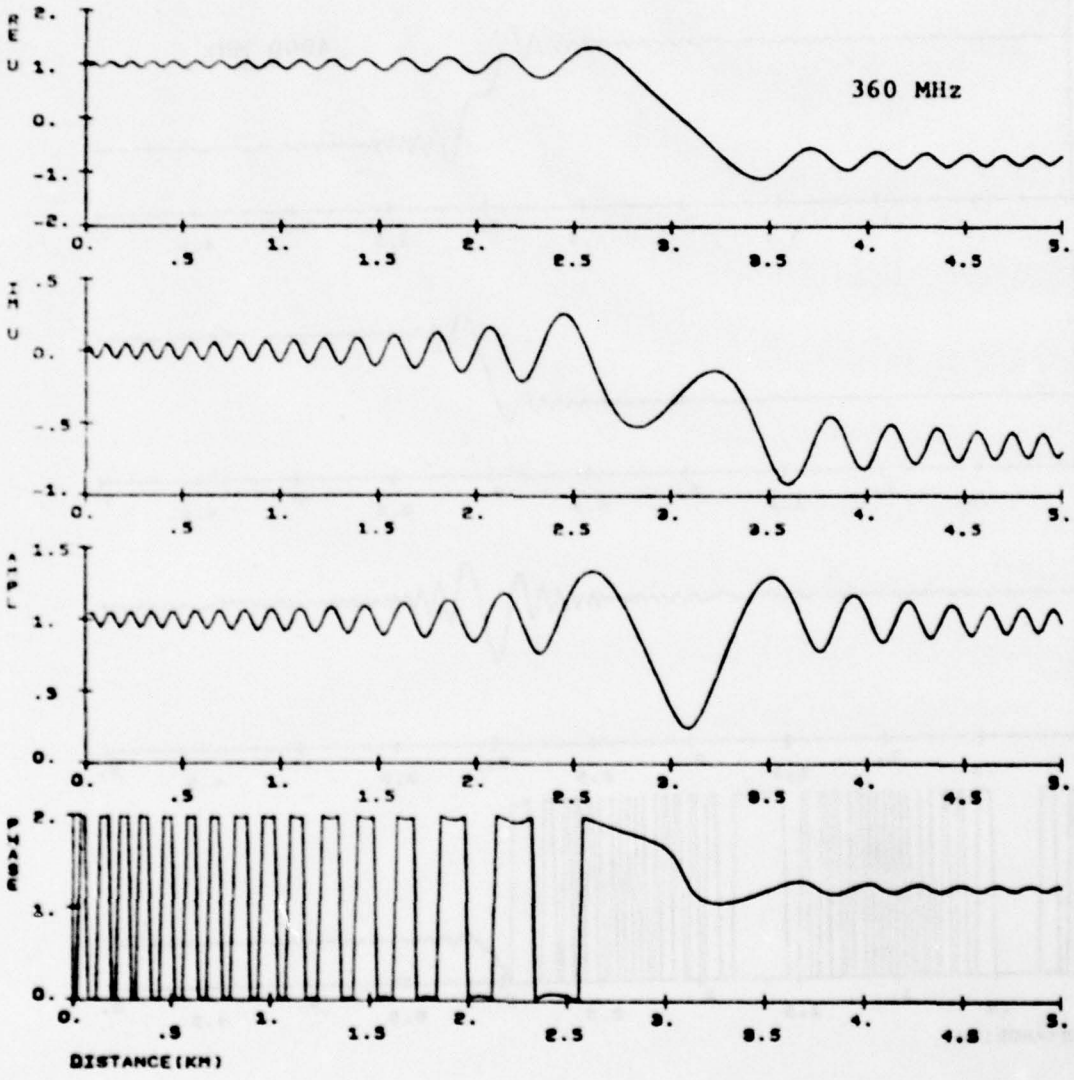
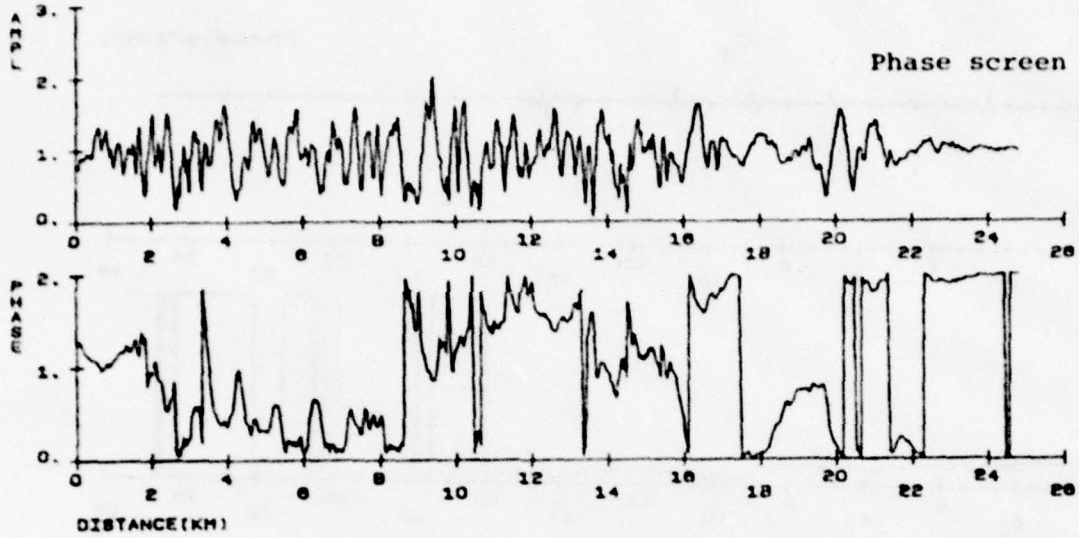
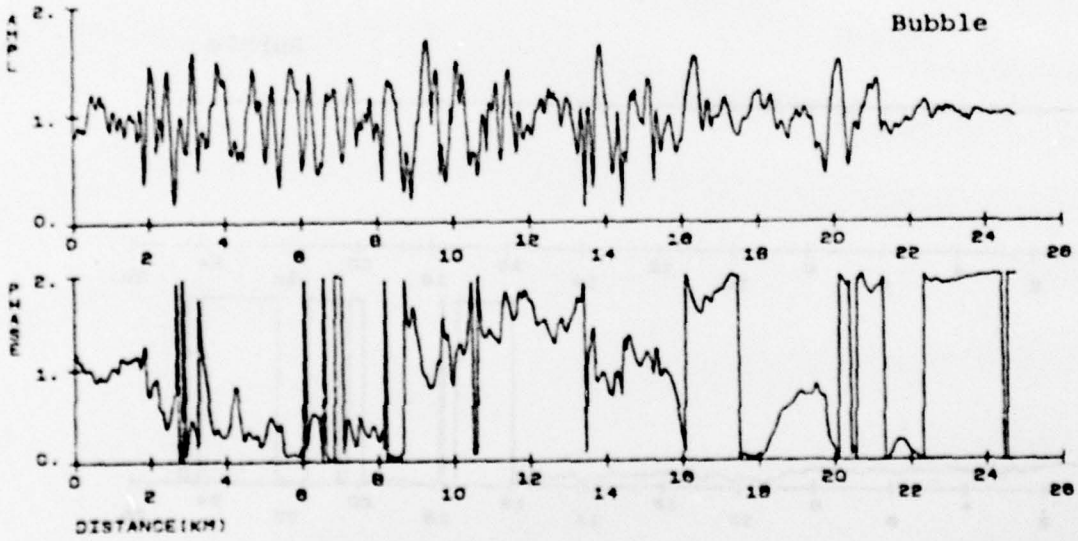


Fig. 9B. Wave structure after passing through a phase screen with discontinuity at a distance 3 km. The phase screen height is 350 km at 360 MHz.

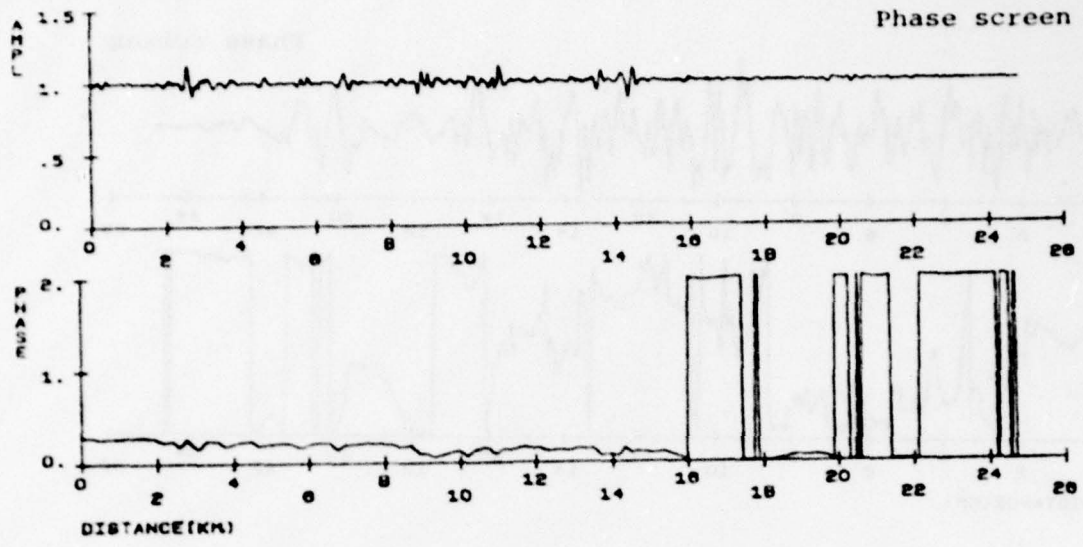


a)

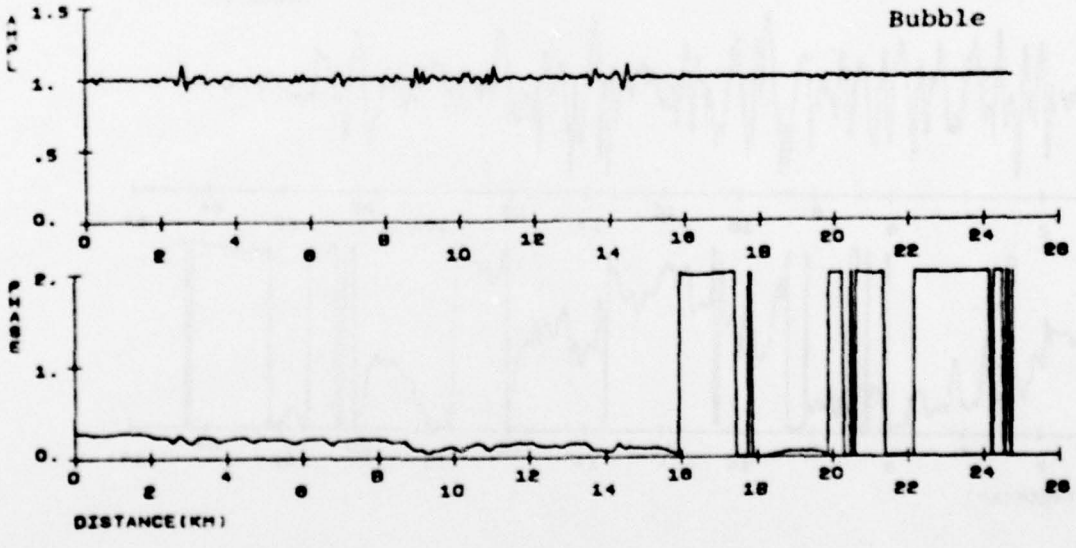


b)

Fig. 10. Comparison of the amplitude and phase pattern at 360 MHz produced by a) a phase screen and b) a bubble.



a)



b)

Fig. 11. The same as in Figure 10 but at 4000 MHz frequency.

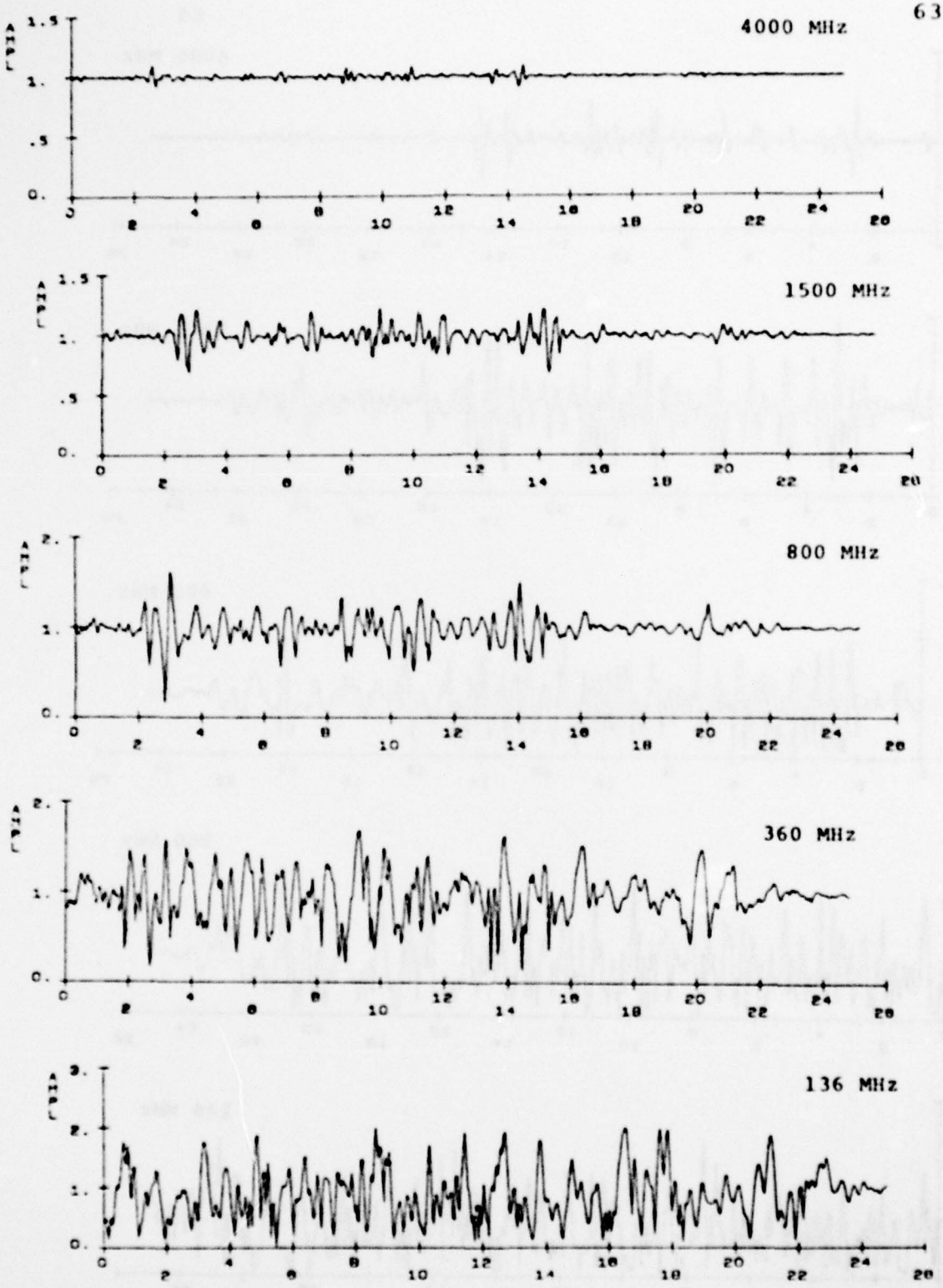


Fig. 12. Amplitude pattern at different frequencies produced by the "initial stage" bubble.

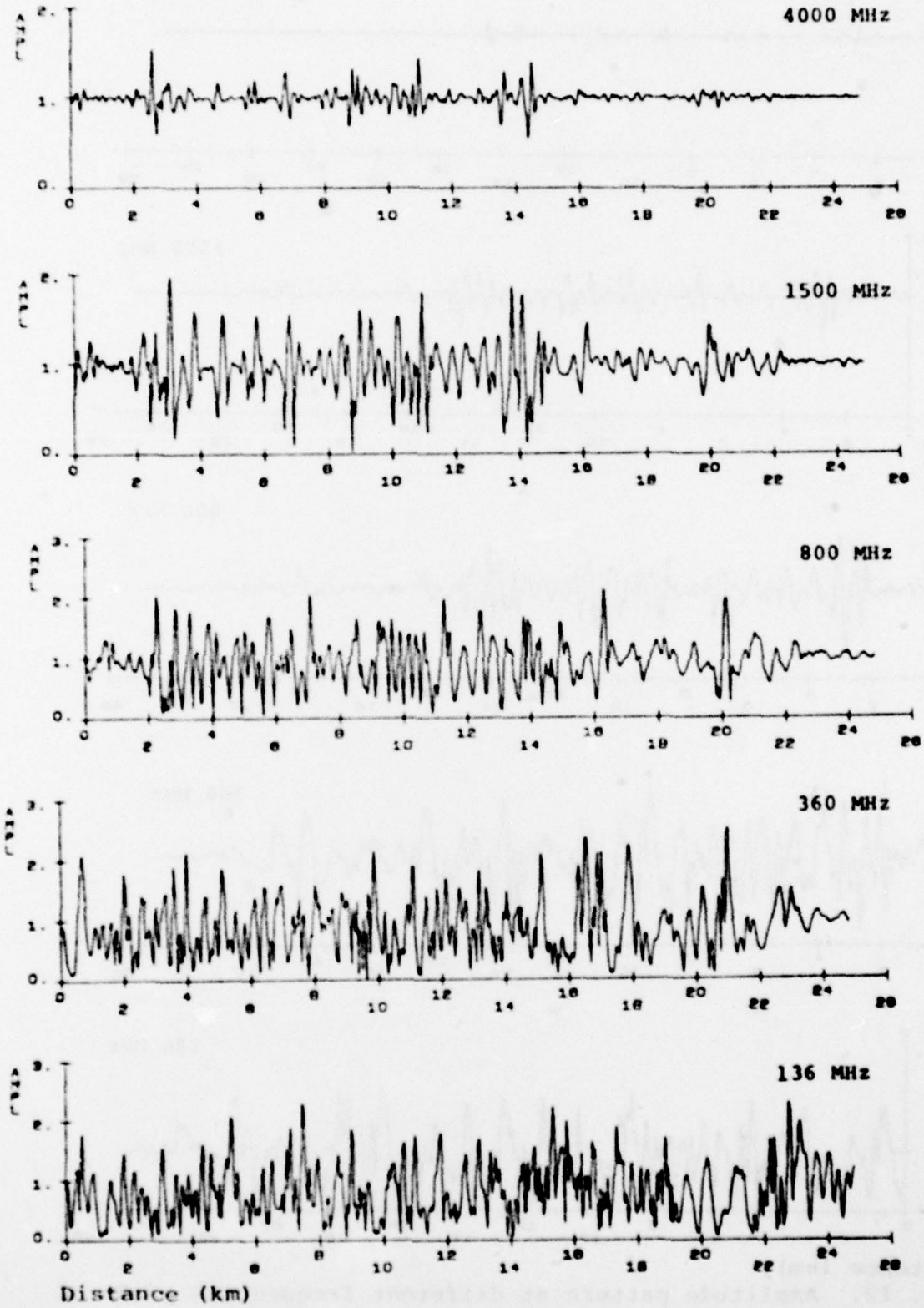


Fig. 13. The same as in Figure 12 but for the "developed stage" bubble.

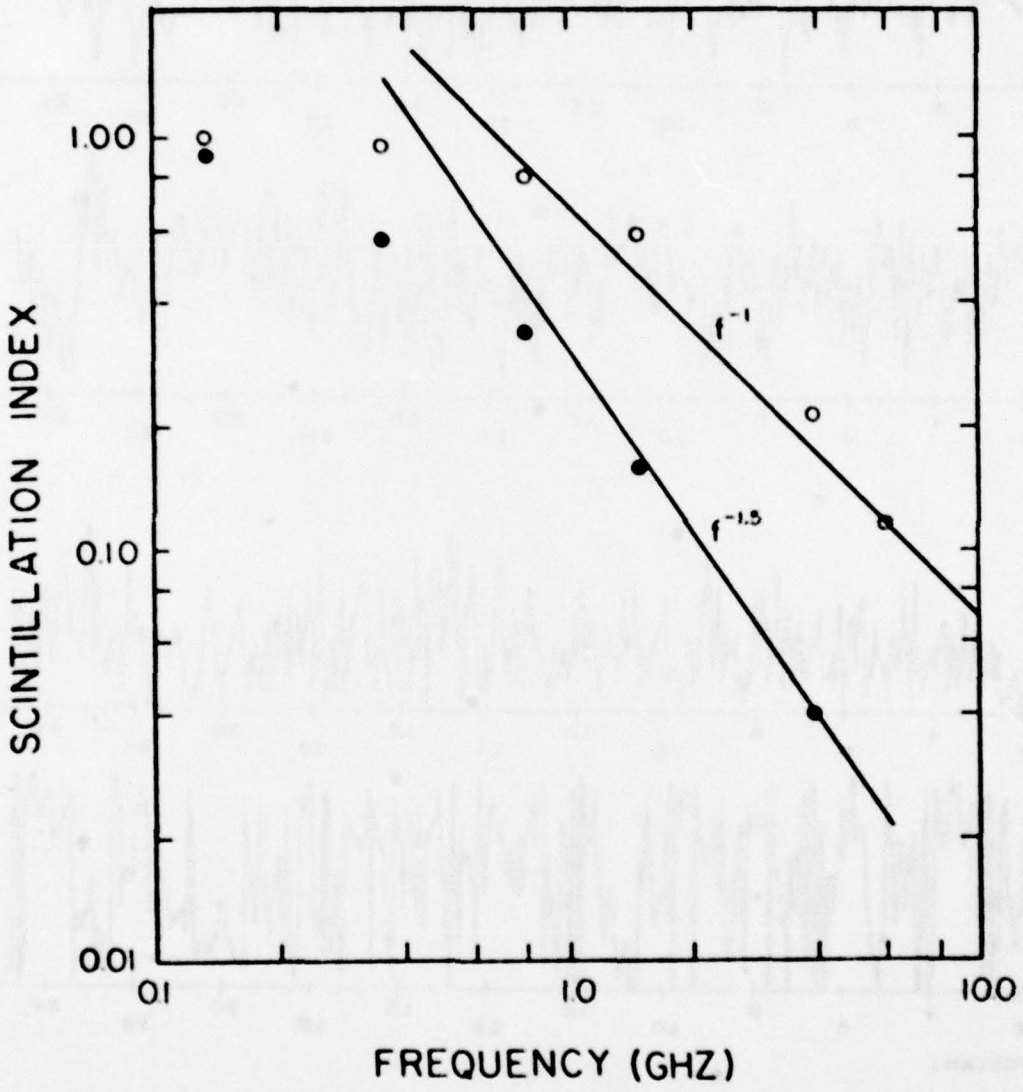


Fig. 14. Scintillation index frequency dependence for the "initial" (dots) and "developed" (open circles) bubble stage.

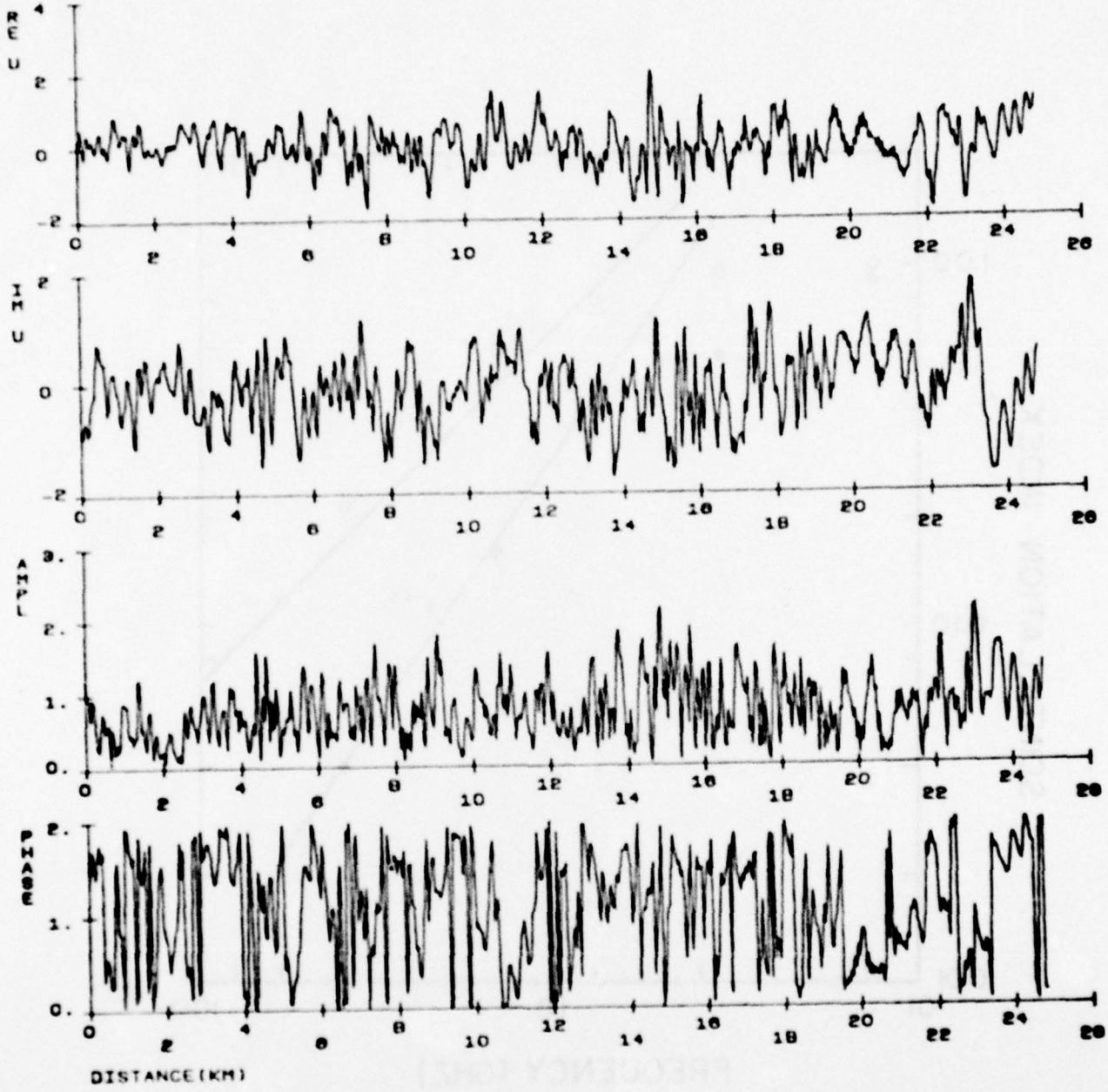


Fig. 15. Wave structure at 136 MHz produced by strong irregularities. Note lower level of the signal close to the center of the bubble.

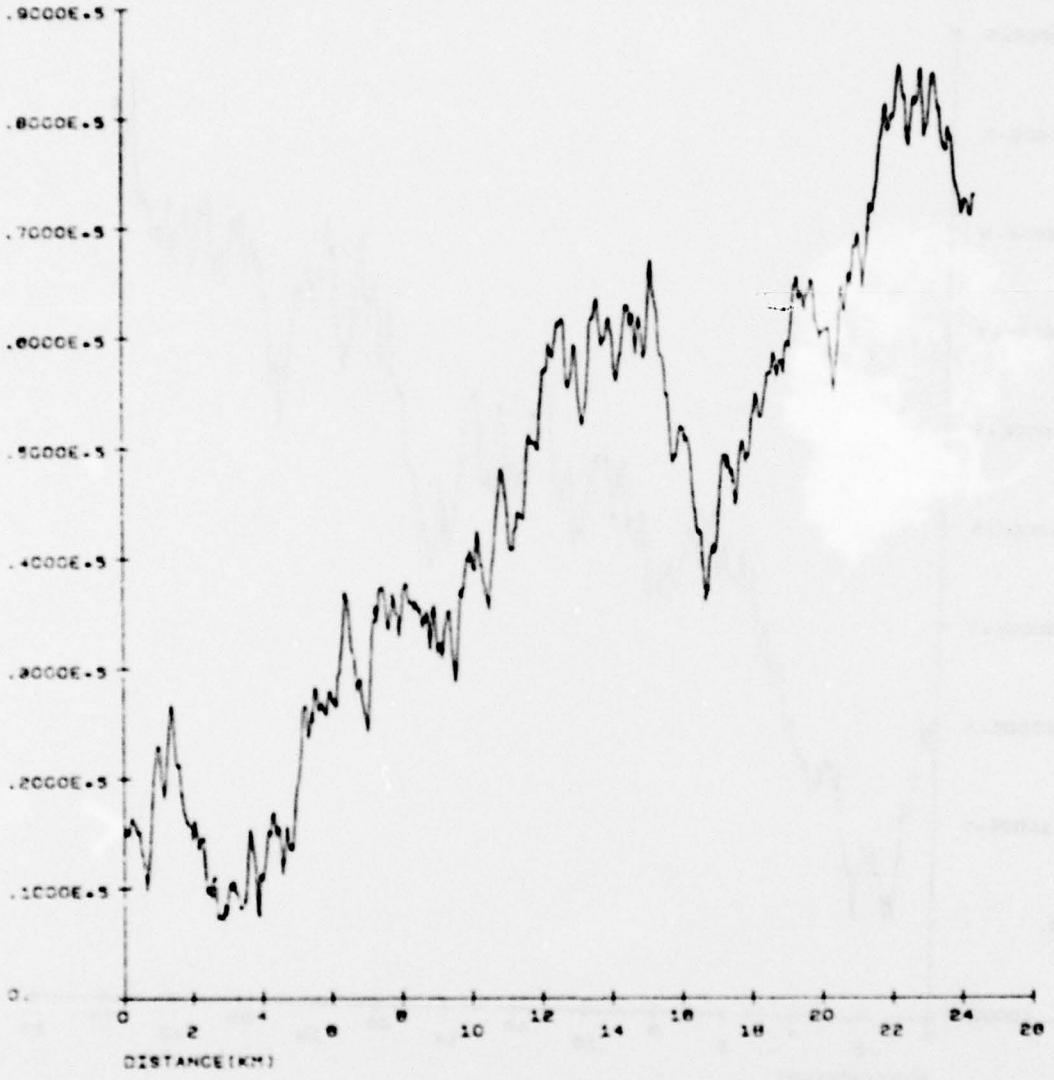


Fig. 16A. Horizontal electron density variations obtained by randomizing phases of the Fourier analyzed high frequency component of the data shown in Figure 1. Run A.

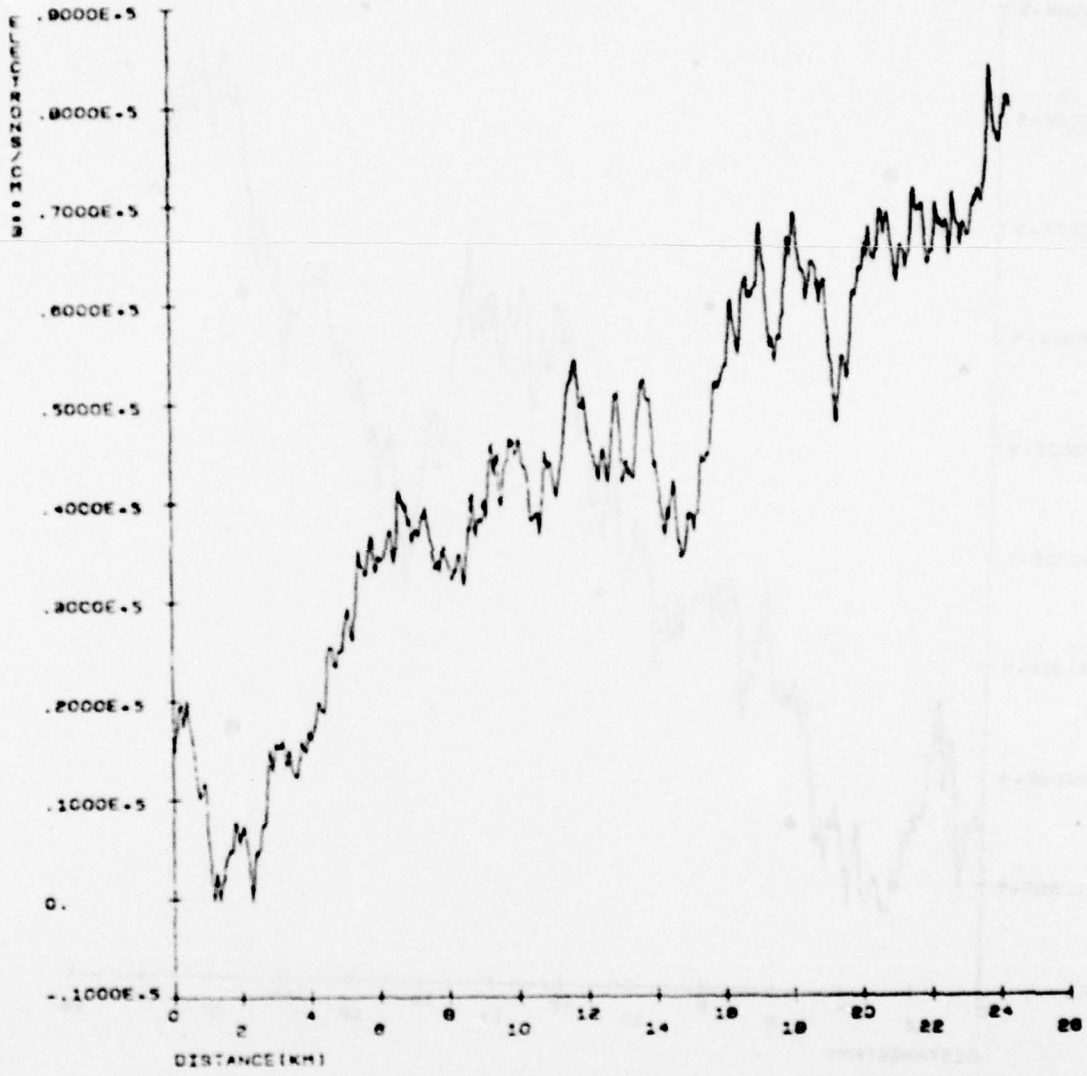


Fig. 16B. Horizontal electron density variations obtained by randomizing phases of the Fourier analyzed high frequency component of the data shown in Figure 1. Run B.

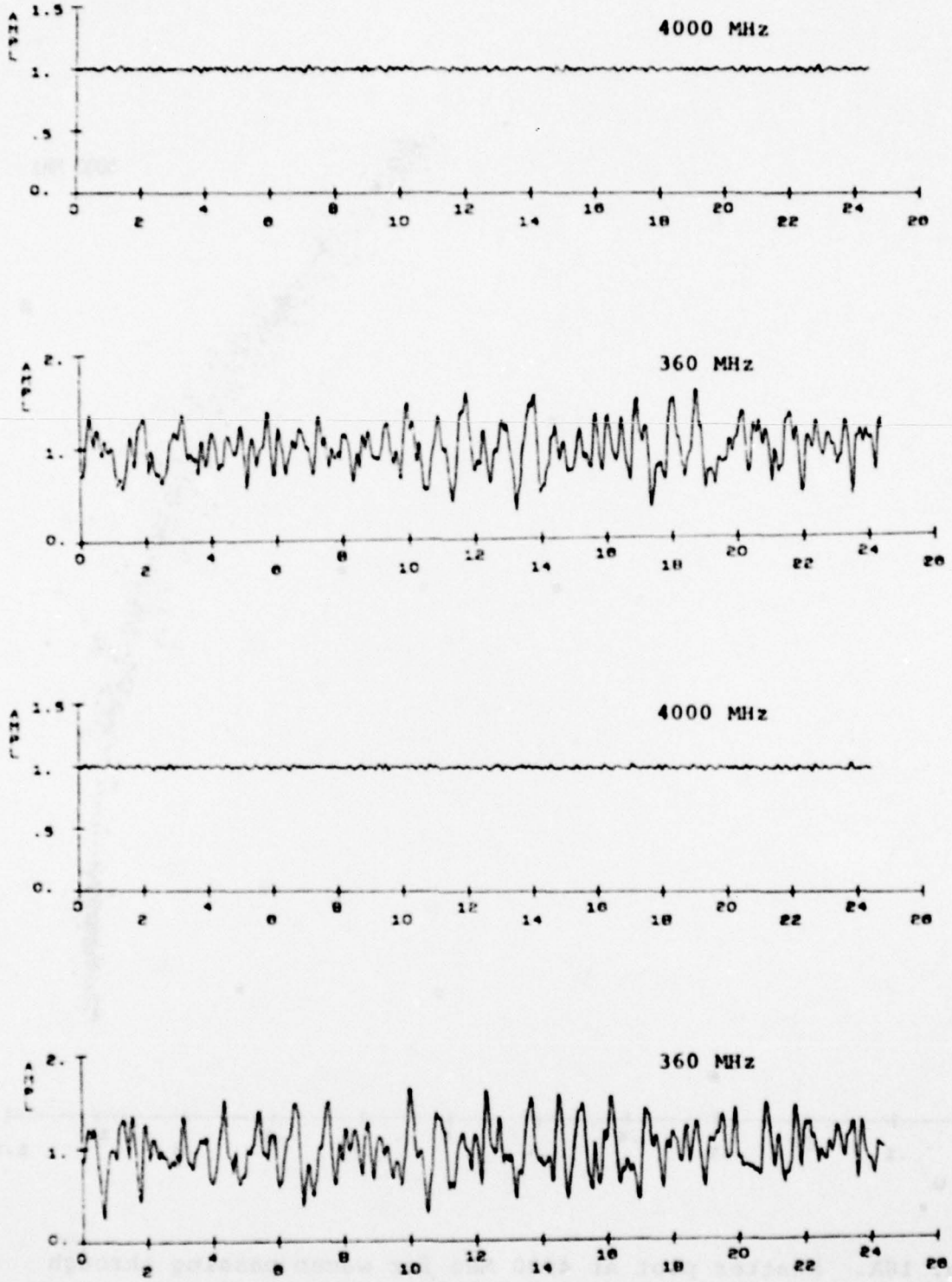


Fig. 17. Amplitude scintillation pattern at 360 MHz and 4000 MHz produced by the "initial stage" bubble with the horizontal structure shown in Figure 16. Two upper panels correspond to run A and two lower panels to run B.

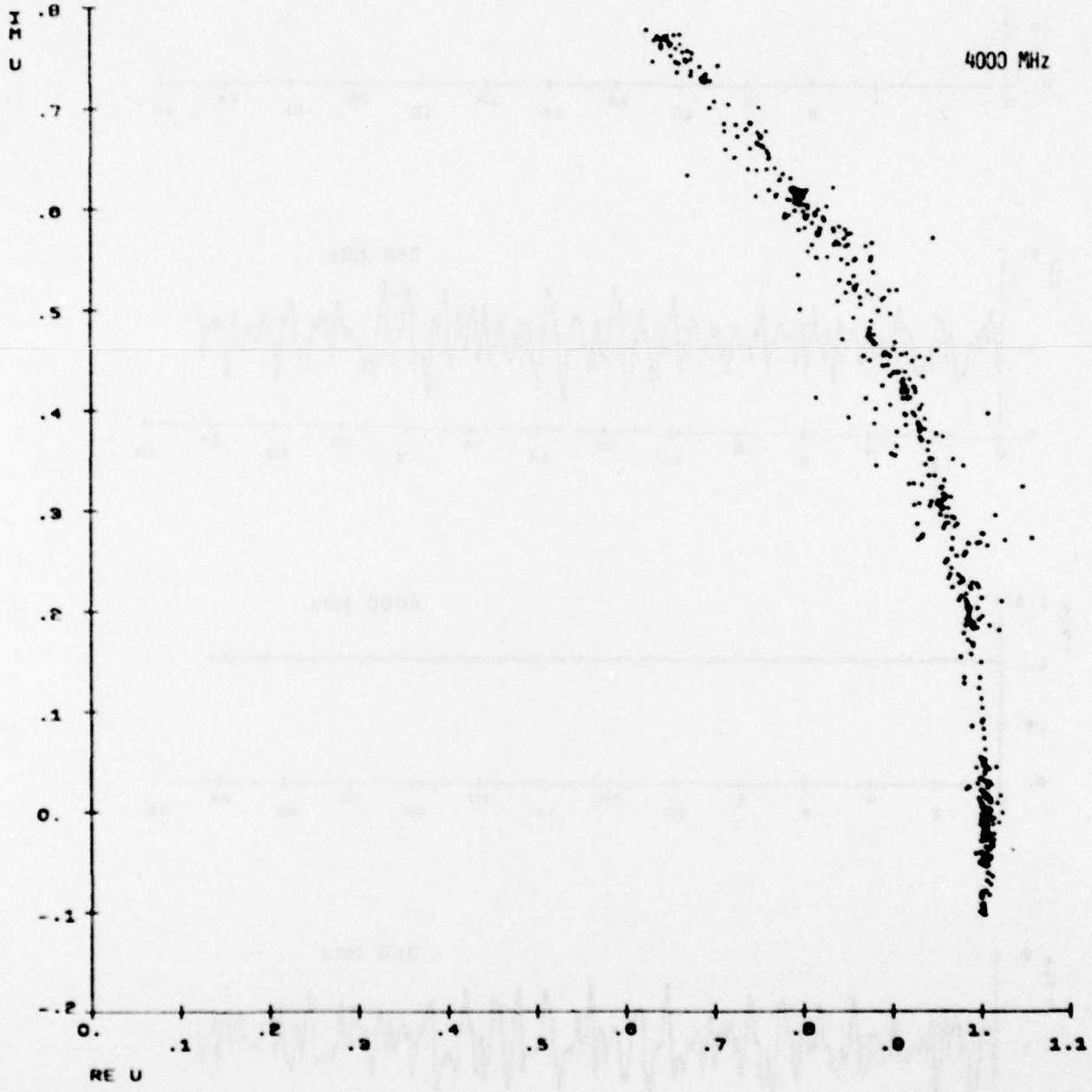


Fig. 18A. Scatter plot at 4000 MHz for waves passing through the "initial stage" bubble.

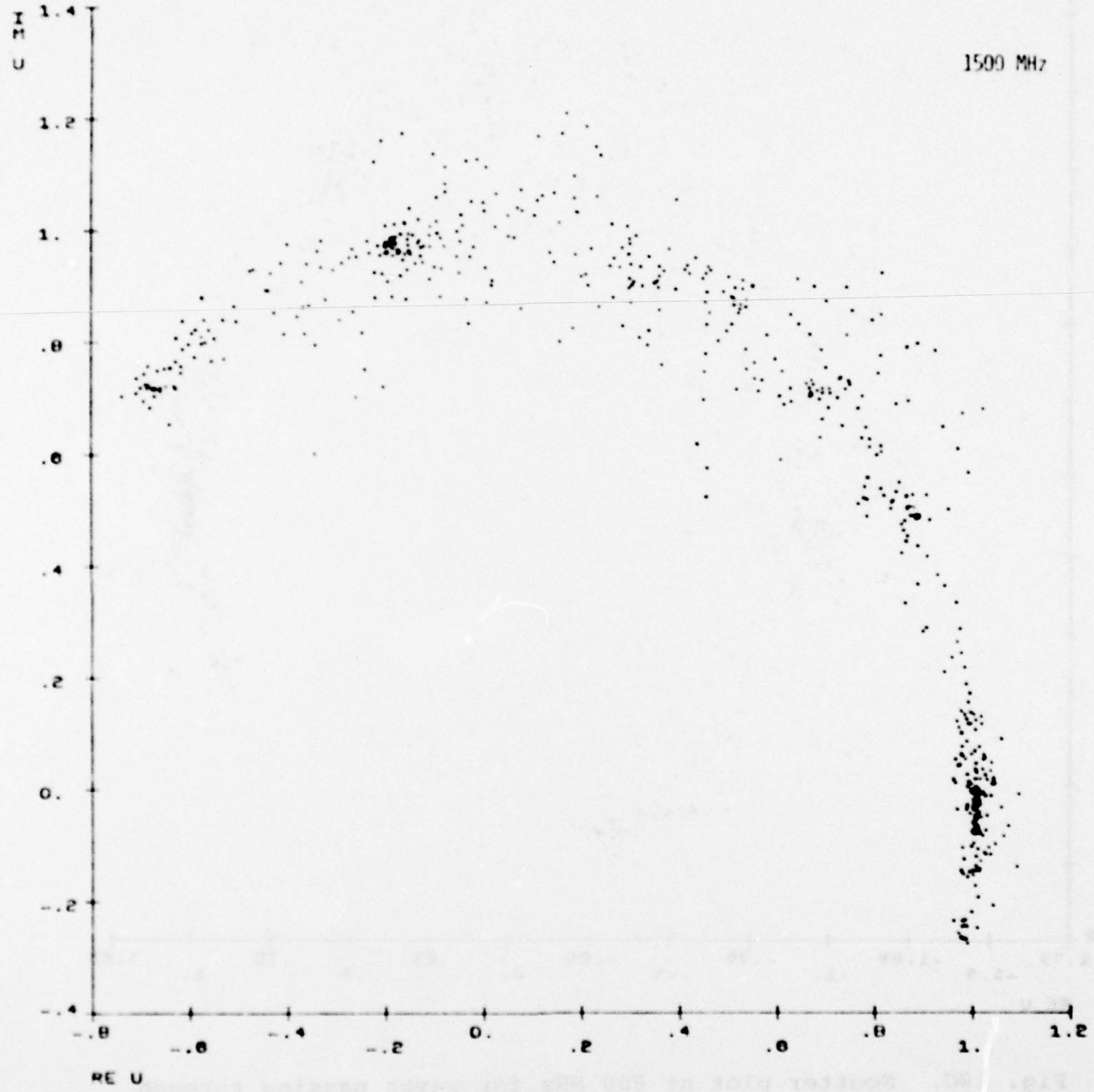


Fig. 18B. Scatter plot at 1500 MHz for waves passing through the "initial stage" bubble.

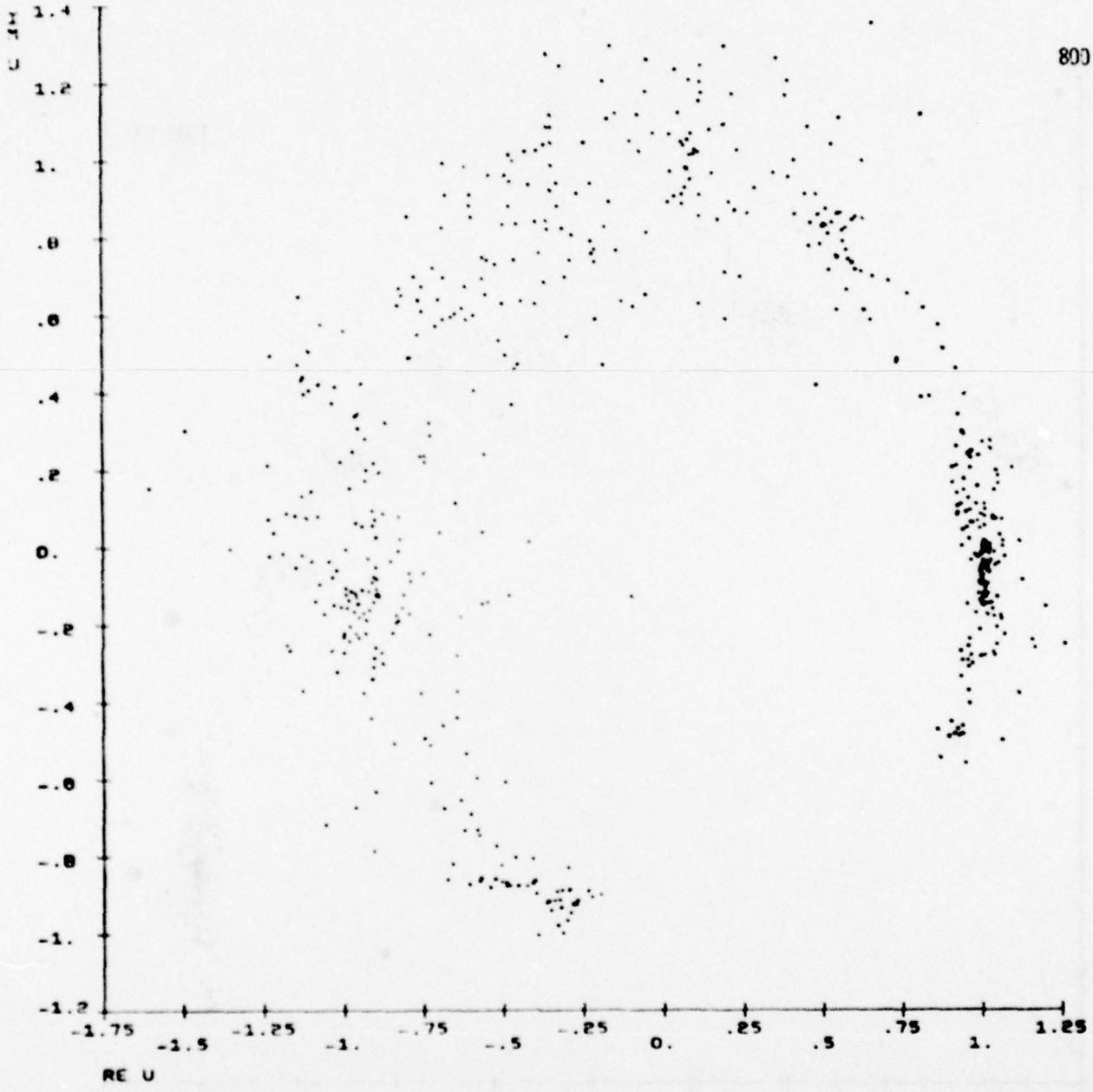


Fig. 18C. Scatter plot at 800 MHz for waves passing through the "initial stage" bubble.

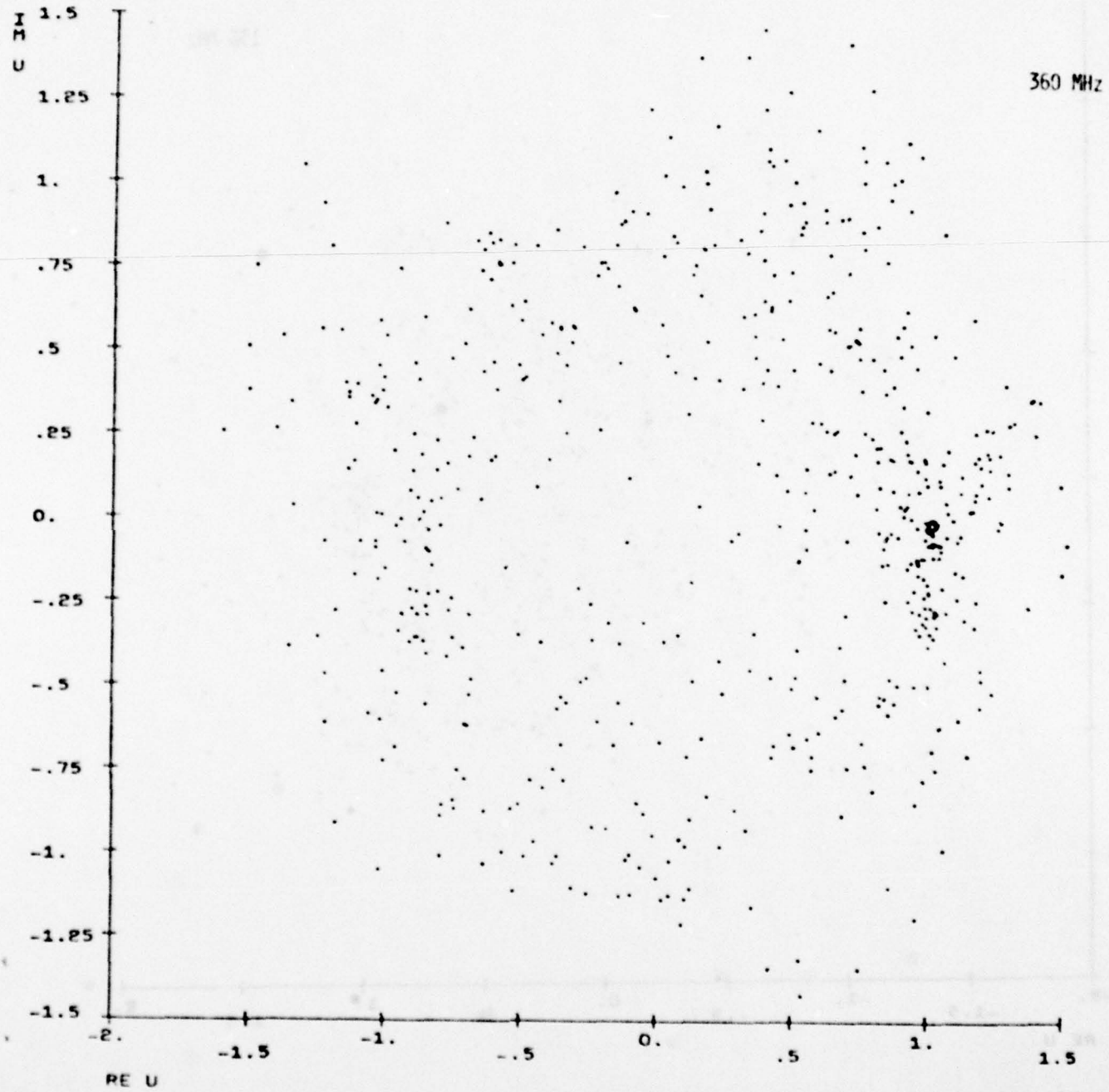


Fig. 18D. Scatter plot at 360 MHz for waves passing through the "initial stage" bubble.

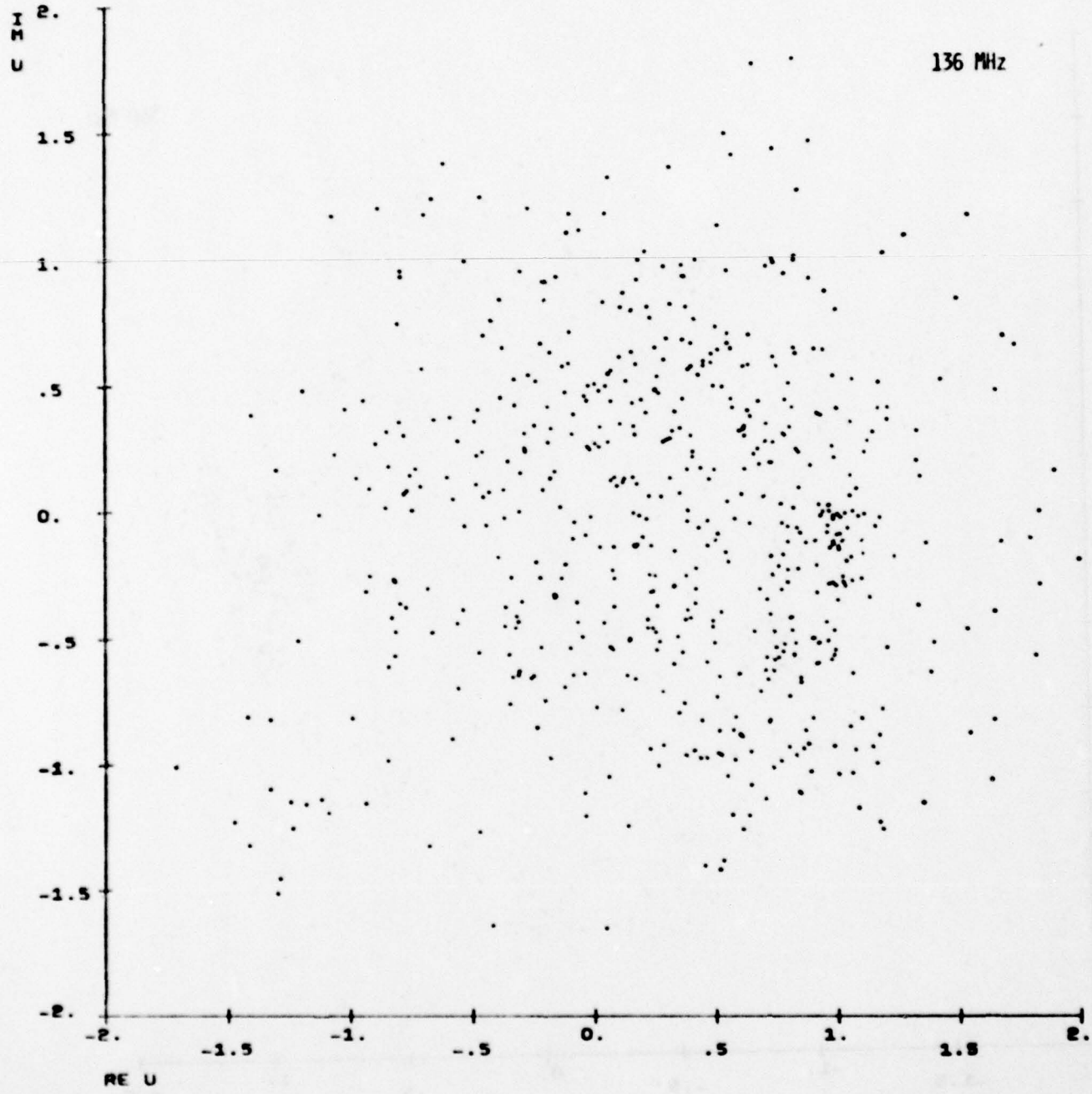


Fig. 18E. Scatter plot at 136 MHz for waves passing through the "initial stage" bubble.